Current Research (2024) Newfoundland and Labrador Department of Industry, Energy and Technology Geological Survey, Report 24-1, pages 53-78

REE PEGMATITES AND THEIR PARENT INTRUSIONS SOUTH OF THE FOX HARBOUR VOLCANIC BELT, SOUTHEASTERN LABRADOR

Z. Magyarosi and N. Rayner[1]
Mineral Deposits Section
[1]Geolocial Survey of Canada, 601 Booth Street, Ottawa, ON, K1A 0E8

ABSTRACT

Rare-earth element (REE) enriched pegmatites occur south of the Fox Harbour Volcanic Belt (FHVB) in southeastern Labrador; the latter representing a 1.31 to 1.27 Ga, ~64-km long, peralkaline to metaluminous belt associated with significant REE mineralization, similar to other Mesoproterozoic peralkaline complexes in Labrador hosting REE mineralization, such as the Strange Lake Complex, Flowers River Igneous Suite and the Red Wine Intrusive Suite. Petrography, scanning electron microscope (SEM) analysis, geochronology, and geochemistry of the pegmatites and their parent intrusions provide new details on the origin of the REE mineralization in the pegmatites and their relationship to the FHVB.

The studied pegmatites are Group 2 (formerly "NYF") pegmatites that are an important economic source of REE and high-field-strength elements (HFSE), many of which are considered critical. The pegmatites occur as dykes, ovoids, lenses, or irregular bodies and are generally less than 1 m wide. The major minerals in the pegmatites include quartz, feldspars, magnetite, titanite, amphibole, pyroxene, biotite and zircon. The main REE minerals are allanite and fergusonite. Other REE and HFSE minerals include monazite, bastnaesite, parisite, synchisite, euxenite, britholite, yttrialite, betafite, thorite and a chevkinite-like mineral. The parent intrusions are granites and syenites consisting of quartz, feldspars, amphibole, pyroxene, biotite, magnetite, titanite, zircon and allanite. Common replacement textures in the pegmatites and parent intrusions indicate that most of the REE and HFSE minerals are at least partially hydrothermal.

The parent granitic intrusions are A-type, mostly metaluminous and formed in a within-plate tectonic setting. Both the pegmatites and parent intrusions are strongly evolved with Zr contents up to ~3 wt. % in the parent intrusions and ~9 wt. % in the pegmatites. The light-rare-earth element (LREE) and heavy-rare-earth element (HREE) enrichments in the parent intrusions are up to ~6000 times and ~1000 times the chondrite values, respectively. The LREE and HREE enrichment in the pegmatites is up to ~20 000 times the chondrite values.

Zircon U–Pb analysis of the pegmatites and their parent intrusions gave igneous crystallization ages of 1311 ± 12, 1310 ± 12, ca. *1260 and 1169 ± 11 Ma. One granite hosting pegmatite gave a crystallization age of 1648 ± 4.8 Ma and was interpreted not to represent a parent intrusion, also suggested by its geochemistry analytics. All samples indicate new zircon growth during the Grenville orogeny around 1.0 Ga.*

Rare-earth element and HFSE mineralization in the pegmatites is the result of magmatic and late-magmatic hydrothermal processes; the latter due to volatiles exsolving from the cooling parent intrusions. The effect of metamorphism on the mineralization is uncertain. Mineralogy, mineral chemistry and geochronology of the pegmatites and parent intrusions suggest that the parent intrusions of the pegmatites may represent the intrusive equivalent of the FHVB. Further exploration should focus on locating additional pegmatites and their parent intrusions with airborne and ground radiometric and magnetic surveys.

INTRODUCTION

This report summarizes the petrography, geochemistry, and geochronology of rare-earth-element (REE) pegmatites and their parent intrusions located south of the Fox Harbour Volcanic Belt (FHVB) in southeastern Labrador (Figure 1). The work is part of a multi-year project funded by the Geological Survey of Newfoundland and Labrador (GSNL) and the Geological Survey of Canada (GSC) through its Targeted Geoscience Initiative (TGI) program. The purpose of the project is to advance the understanding of the genesis of REE mineralization hosted in alkaline–peralkaline systems.

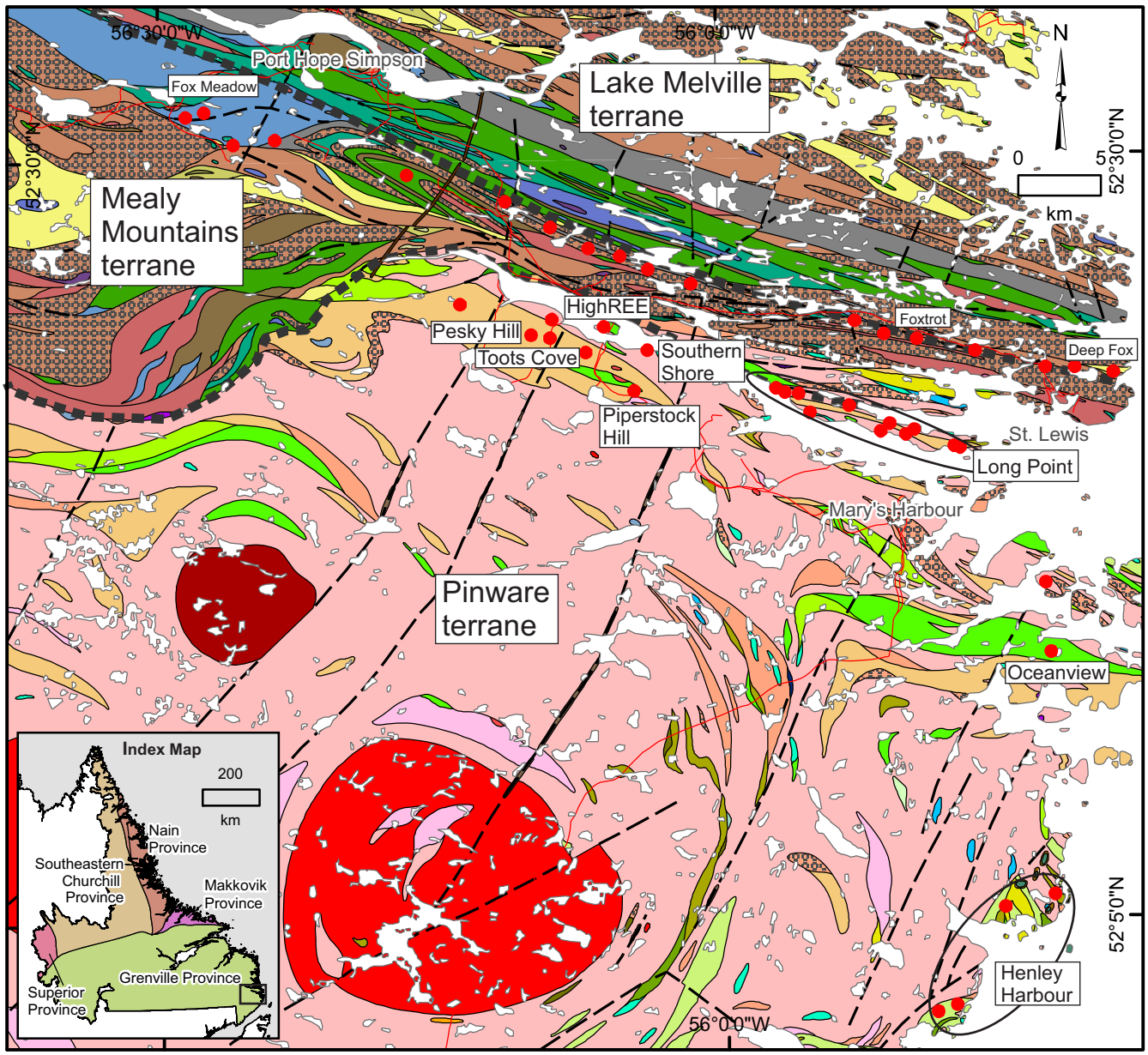

Figure 1. *Geology of the Port Hope Simpson area, southeastern Labrador (after Gower, 2010a, b, 2019). The east-northeast trending line of REE occurrences from Deep Fox to Fox Meadow outlines the Fox Harbour Volcanic Belt (FHVB). Study area indicated by the outlined black box on the index map.*

The FHVB is a 1.31–1.27 Ga peralkaline complex (Haley, 2014; Magyarosi and Rayner, 2023) and is similar to other REE mineralized Mesoproterozoic peralkaline complexes in Labrador, including the Strange Lake Complex, the Flowers River Igneous Suite as well as the Red Wine Intrusive Suite (Miller *et al.*, 1997; Crocker, 2014; Ducharme *et al.*, 2021). These deposits are enriched in both heavy-rare-earth elements (HREE) and light-rare-earth elements (LREE), and this type of deposit may be more beneficial for REE mining and processing compared to the REE deposits hosted in ionic clays and carbonatites (Dostal, 2016; Goode, 2021).

Rare-earth-element mineralization in the FHVB and the pegmatites to the south was discovered by Search Minerals Incorporated in 2010. Most of the exploration concentrated on the Deep Fox, Foxtrot and Fox Meadow occurrences along the FHVB (Figure 1). The resources at Deep Fox and Foxtrot were recently updated by Ciuculescu *et al.* (2022). This paper concentrates on the REE pegmatites and their parent intrusions to the south and their potential relationship to the FHVB. For more details on the geology of the FHVB, *see* Miller (2015) and Magyarosi and Rayner (2023).

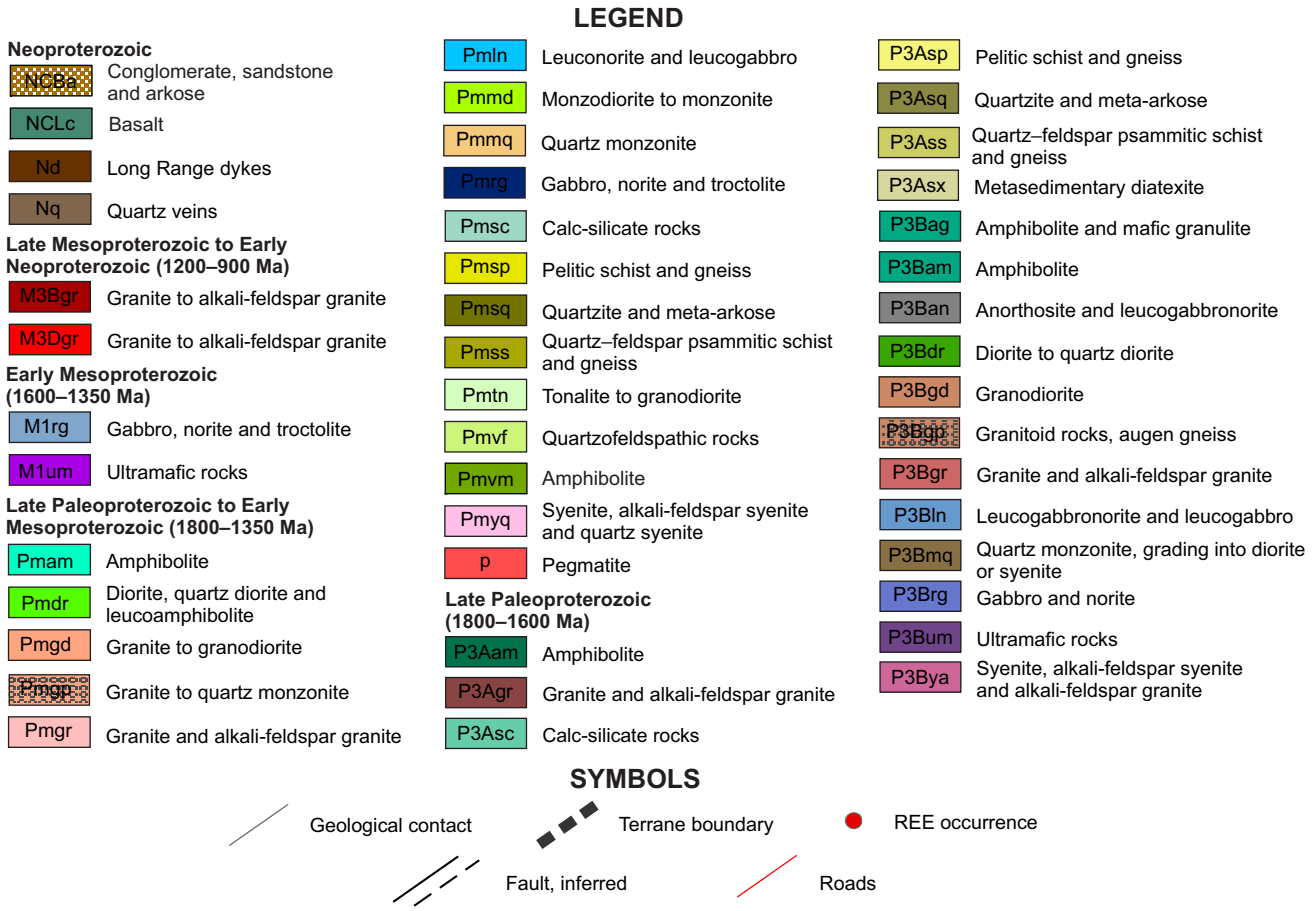

Figure 1. *Legend.*

REE PEGMATITES

Pegmatites are igneous rocks characterized by variable textures, diverse mineralogy, and extreme chemical compositions (Wise *et al.*, 2022; Müller *et al.*, 2023). They may be associated with a parent plutonic rock where they form in the final stages of magma crystallization, or they may form as a result of anatexis in metamorphic rocks. Granitic pegmatites are the most common, but they may be associated with any type of plutonic rocks (*e.g.*, syenite, gabbro). Pegmatites are rich in incompatible elements that do not easily fit in the crystal structure of common rock-forming minerals; including REE, HFSE, Li, Be and volatiles (F, Cl, CO_2, and P) and are an important economic source of these elements, most of which are considered critical (https://www.gov.nl.ca/iet/files/Critical-Minerals-Plan-Our-Critical-Minerals-Advantage.pdf).

Recent research (Wise *et al.*, 2022) proposed subdividing granitic pegmatites, based on their mineralogy into Group 1, Group 2 and Group 3 pegmatites; formerly known as lithium–cesium–tantalum (LCT), niobium–yttrium–fluorine (NYF), and "hybrid" pegmatites, respectively. The pegmatites south of the FHVB are classed as Group 2 pegmatites; most commonly associated with A-type intrusions ranging from peralkaline to metaluminous and mildly peraluminous and occurring in post-orogenic or anorogenic settings. These pegmatites are hosted within, or close to, their parent intrusions, if there is one, and are rich in REE, HFSE, Be and F. Minerals in this group may include magnetite, titanite, uraninite, sodic to calcic amphibole and pyroxene, fayalite, allanite, gadolinite, monazite, euxenite, fergusonite, amazonite, fluorite, beryl and topaz. They are magnetic and have high scintillometer counts, due to the presence of magnetite and U- and Th-bearing minerals, making them relatively easy exploration targets. The Group 2 pegmatites are further subdivided into three types: 1) those enriched in Fe-minerals (biotite, fayalite, Na-rich amphibole); 2) those containing magnetite, uraninite and REE-bearing oxides and silicates; and 3) those characterized by elevated Be and F contents containing beryl, topaz and fluorite (Wise *et al.*, 2022). The pegmatites in the study area are a mixture of the first and second types, both of which are characterized by various degrees of enrichment

in REE and HFSE. Other examples of these types of pegmatites include Strange Lake in northern Labrador and Québec and the Pikes Peak batholith in Colorado (Wise *et al.*, 2022).

GEOLOGICAL SETTING

The Grenville Province in eastern Labrador is composed of late Paleoproterozoic to Mesoproterozoic rocks formed *via* multiple orogenic and related events including the Eagle River (1810–1775 Ma), Labradorian (1710–1600 Ma), Pinwarian (1520–1460 Ma) orogeneses, post-Pinwarian–pre-Grenvillian events (1460–1090 Ma), Grenvillian orogenesis (1090–920 Ma) and Neoproterozoic and Phanerozoic events (Figure 1; Gower, 2019). It is subdivided into five terranes, namely, from north to south: the Groswater Bay, Hawke River (not shown on figure), Lake Melville, Mealy Mountains and Pinware terranes (Figure 1; Gower, 2019). The terranes are distinguished from one another based on the type and degree of deformation and metamorphism they underwent during each orogenic event. The Mealy Mountains terrane is distinguished from the Pinware terrane by the presence of significant pre-Pinwarian history. The Lake Melville terrane went through severe Grenvillian deformation, whereas the Mealy Mountains and Pinware terranes were only moderately affected by Grenvillian orogenesis (Gower, 2019).

The REE pegmatites and their parent intrusions south of the FHVB are located in the Pinware terrane, whereas the FHVB is located in the Mealy Mountains terrane, straddling the boundary with the Lake Melville terrane to the north (Figure 1). The oldest units in the Pinware terrane are late Paleoproterozoic (1810–1600 Ma). In the western Pinware terrane, these are composed of supracrustal rocks, foliated and gneissic granitoids and mafic rocks, whereas in the Henley Harbour district in the east, they are composed of amphibolite, quartzofeldspathic rocks, quartzite, tonalitic gneiss, pelitic and calc-silicate rocks. Foliated gneissic granitoids and minor mafic rocks underlie most of the Pinware terrane (Figure 1). Late Mesoproterozoic to Neoproterozoic rocks are subdivided into late- to syn-Grenvillian granitoid intrusions (1045–985 Ma), early- to post-Grenvillian granitoid and minor mafic intrusions (985–975 Ma) and late- to post-Grenvillian granitoid intrusions (975–955 Ma). Phanerozoic rocks occur in the southeast, along the shoreline, and consist of clastic sedimentary rocks and minor limestone.

The area south of the FHVB has been mapped at 1:100 000 scale (Gower, 2019); no detailed maps of the pegmatites and their parent intrusions exist.

ANALYTICAL METHODS

Two hundred and fourteen samples were collected in the summer of 2021 and 2022 from the Henley Harbour (39), Oceanview (31), HighREE (83), Southern Shore (10), Piperstock Hill (10), Pesky Hill (17), Toots Cove (8) and Long Point (16) occurrences (Figure 1). The samples included pegmatites, their host rocks, and other rocks in spatial proximity. Whole-rock geochemical analyses were completed at the geochemical laboratory of the GSNL. Samples were cleaned, crushed, pulverized, and analyzed according to Finch *et al.* (2018). Polished thin sections of representative samples were examined using a petrographic microscope. The results of the geochemical analysis are published in Magyarosi (2023).

Fifteen samples of pegmatites (3 from Henley Harbour, 3 from Oceanview, 4 from HighREE, 1 from each of Southern Shore, Piperstock Hill, Pesky Hill, Toots Cove and Long Point) were selected for analysis using a FEI MLA 650FEG scanning electron microscope (SEM) at the Memorial University of Newfoundland Micro Analysis Facility (MUN MAFIIC). Qualitative analyses were completed using high throughput Energy-dispersive X-ray Spectroscopy (EDX) detectors from Bruker (https://www.mun.ca/creait/). The purpose of the SEM work was to identify the unknown minerals (as many as possible) and provide qualitative compositions of amphiboles and pyroxenes in the pegmatites.

Age determinations of six samples (1 from Henley Harbour, 1 from Oceanview, 1 from Pesky Hill, 2 from HighREE and 1 from Long Point) were undertaken at the Geochronology Laboratories at the Geological Survey of Canada in Ottawa. The samples were disaggregated using standard crushing/pulverizing techniques followed by density separation using the Wilfley table and heavy liquids, followed by magnetic separation (unless otherwise noted). Grains selected for Sensitive High Resolution Ion Microprobe (SHRIMP) analysis, were cast in epoxy mounts IP1005, 1029 and 1031. The mid-sections of the minerals were exposed through polishing with diamond compound, and internal features characterized in cathodoluminescence (CL) and back-scattered electron (BSE) mode utilizing a TESCAN Mira3 SEM. Mount surfaces were evaporatively coated with 10 nm of high purity Au. SHRIMP analytical procedures followed those described by Stern (1997). Fragments of the Temora2 primary zircon reference material (RM) (GSC lab number 10493; $^{206}Pb/^{238}U$ age = 416.5 ± 0.22 Ma, Black *et al.*, 2004) and secondary zircon RMs 6266 ($^{206}Pb/^{238}U$ age = 559 ± 02 Ma, Stern and Amelin, 2003), 1242 ($^{207}Pb/^{206}Pb$ age = 2679.7 ± 0.2 Ma, Davis *et al.*,

2019) and 9910 (441.2 ± 0.4 Ma, B. Davis and V. McNicoll, unpublished data, 2010) were analyzed on the same mount and under the same conditions as the unknowns. Analyses were conducted using an O− primary beam, with a spot size of either 20 or 10 μm at a beam current between 3–8 nA. The count rates of the isotopes of U, Th and Pb as well as Hf and Yb for zircon were sequentially measured over six scans with a single electron multiplier. Offline data processing was accomplished using Squid3 (Bodorkos *et al.*, 2020) software. Decay constants used follow the recommendations of Steiger and Jäger (1977). The 1σ external errors of $^{206}Pb/^{238}U$ ratios reported in the data table (Appendix A) incorporate a ± 0.8% uncertainty in calibrating the primary RM (*see* Stern and Amelin, 2003). Analyses of a secondary zircon RM 1242 were interspersed between the sample analyses to assess the requirement of an isotopic mass fractionation correction for the $^{207}Pb/^{206}Pb$ ages; however, none was required. Details of the analytical session (mount/session number, spot size, primary beam intensity) are recorded in the footnotes of the data table as are the measured weighted mean age for the secondary RMs for that session (Appendix A). Common Pb correction utilized the measured $^{207}Pb/^{206}Pb$ ratios and common Pb compositions modelled after Stacey and Kramers (1975). Isoplot *vs.* 4.15 (Ludwig, 2012) was used to generate concordia plots and calculate weighted means. If the zircon population of interest consists of dates older than 1500 Ma, the weighted mean $^{207}Pb/^{206}Pb$ age is reported, if younger, the $^{206}Pb/^{235}U$ age is reported. This threshold, albeit arbitrary, is selected based on the approximate inflexion point of the relative precision of the two ages when determined by SHRIMP. The error ellipses on the concordia diagrams and the weighted mean errors are reported at 95% confidence, unless otherwise noted. An evaluation of the long-term reproducibility of $^{206}Pb/^{238}U$ age of secondary standard 9910 indicates that the minimum precision of SHRIMP ion probe weighted mean results is ± 0.8% (2σ, B. Davis, pers. comm., 2023). In cases where the precision of the weighted mean age calculation for individual samples falls below this threshold, the weighted mean 2σ uncertainty is augmented to 0.8%. Uncertainties reported in the data table (Appendix A) are given at the 1σ confidence interval.

RESULTS

FIELD OCCURRENCE AND PETROGRAPHY

Pegmatites

The pegmatites south of the FHVB occur as dykes (Plate 1A), ovoid shapes (Plate 1B), lenses (Plate 1C) or irregular bodies. The size of the pegmatites varies up to ~5 m in thickness, but they are generally less than 1 m wide. Grain size ranges from fine to very coarse grained. Some of the pegmatites are zoned (Plate 1A, D–F), but most are irregular or patchy with no clear zoning. Examples of zoning include K-feldspar-rich, very coarse-grained border zones and quartz ± magnetite ± pyroxene cores (Plate 1A) or *vice versa* (Plate 1F), fine-grained, albite-rich border and coarser K-feldspar-rich core, and allanite-rich pockets surrounded by magnetite ± pyroxene-rich border zones (Plate 1E). The pegmatites can be subdivided into three main types: 1) magnetite- and/or pyroxene-rich (Plate 2A, B); 2) biotite and/or amphibole-rich (Plate 2C, D); and 3) containing wisps of fine-grained zircon (Plate 2E); although there is significant overlap among the groups. Type 1 pegmatites are most common in the Henley Harbour area, Type 2 pegmatites are most common in the Oceanview area, and Type 3 pegmatites only occur in the HighREE area, but most areas contain a mix of Type 1 and Type 2 pegmatites.

The minerals composing the pegmatites include quartz, K-feldspar, plagioclase, magnetite/titanomagnetite, ilmenite, rutile, zircon, titanite, amphibole, pyroxene, biotite, apatite, fluorite, calcite, galena, sphalerite and REE and HFSE minerals listed in Table 1. The K-feldspar is microcline and is commonly replaced by albite (Plate 3A). The plagioclase in all pegmatites is predominantly albite, except one pegmatite, which displays zoned plagioclase having a Ca-rich core and Na-rich rim. Ferromagnesian minerals include pyroxene, amphibole and biotite, occurring in most pegmatites. Pyroxene is more common at Henley Harbour, whereas amphibole and biotite are more common at Oceanview; most areas contain all three minerals in variable proportions. In several pegmatites, there is evidence of amphibole replacing pyroxene (Plate 3B) and biotite replacing amphibole (Plate 3C). SEM-EDX analysis indicate that the pyroxene and amphibole are rich in Ca and Fe, but also contain Na, Mg and, in amphibole, K. These compositions are similar to the amphiboles and pyroxenes in the FHVB, where the amphiboles are calcic to calcic–sodic and less commonly sodic and K-bearing, and the pyroxenes are aegirine–augite (ZM, unpublished data, 2024).

The most common REE minerals are allanite and fergusonite, which typically occur with titanite, magnetite, zircon, thorite and other REE minerals. Allanite is typically zoned and patchy (Plate 3D–F). In some of the pegmatites, allanite contains remnants of titanite and locally a chevkinite-like mineral, suggesting that allanite and chevkinite replaced titanite (Plate 3E). In other examples, REE-rich allanite is replaced by REE-poor allanite and bastnaesite (Plate 3G). Allanite also commonly contains inclusions of thorite, and in one pegmatite from Oceanview, it surrounds a core of apatite containing abundant thorite (Plate 3H). Fergusonite is also commonly zoned with a darker core and lighter rim (Plate 4A, B). Fergusonite in pegmatites from Oceanview locally surround and replace zircon (Plate 4C,

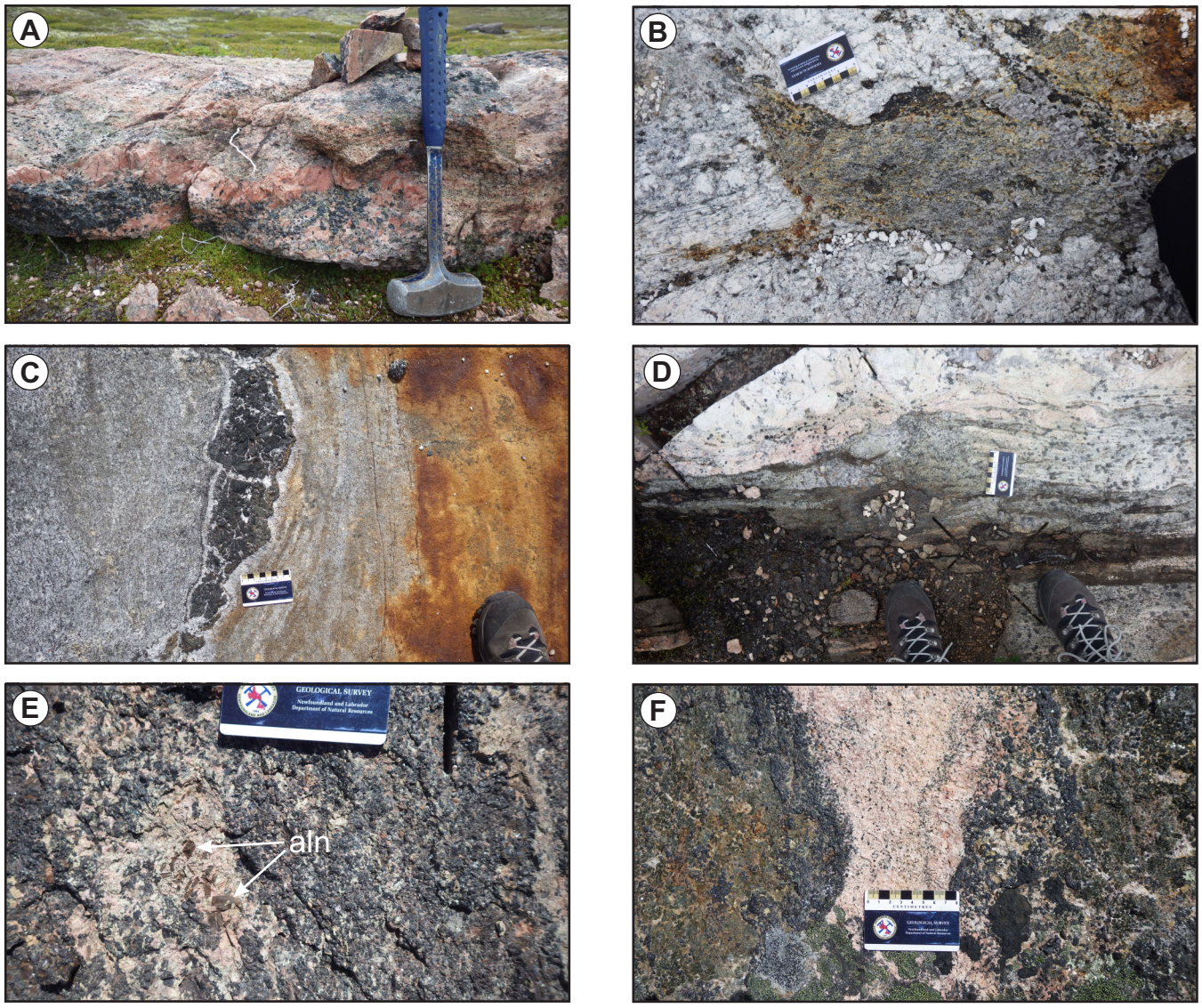

Plate 1. *Field photos of pegmatites. A) Zoned pegmatite dyke at Henley Harbour: K-feldspar-rich very coarse-grained border zone and quartz, magnetite and pyroxene core; B) Ovoid-shaped pegmatite at Pesky Hill; C) Lens-shaped pegmatite at Toots Cove; D) Zoned pegmatite dyke at Oceanview; E) Allanite-rich pocket surrounded by magnetite and pyroxene-rich border zone at Henley Harbour; F) Zoned pegmatite at Henley Harbour: K-feldspar-rich core and quartz ± magnetite ± pyroxene border zone. (Abbreviations* see *Whitney, 2010.)*

D), amphibole (Plate 4E), biotite (Plate 4F) and titanite (Plate 4G), suggesting that it crystallized after them. When occurring with allanite, fergusonite commonly surrounds allanite, suggesting that some of the fergusonite crystallized after allanite (Plate 4A). Fergusonite commonly contains abundant inclusions of galena (Plate 4D).

Less common REE minerals include monazite, euxenite, bastnaesite, synchisite, parisite, britholite, yttrialite and a chevkinite-like mineral. Monazite was only observed at Oceanview and Long Point, although it may have been overlooked in the other areas due to its similarity to zircon. At Oceanview, it occurs with allanite surrounding zircon, whereas at Long Point, it is associated with euxenite, fergusonite, bastnaesite and thorite; commonly surrounding thorite (Plates 4H and 5A). Euxenite was only found at Long Point where it forms grains up to 4 mm long (Plates 4H and 5A). Rare-earth-element fluorocarbonates include bastnaesite (Plates 3G and 5A, B), synchisite (Plate 5C) and parisite. They typically occur late, replacing earlier minerals such as amphibole (Plate 5B), allanite (Plate 3G) and fergusonite. Britholite is less common, but also occurs late, replacing allanite. The chevkinite-like mineral is associated with allanite and titanite (Plate 3E), bastnaesite, monazite

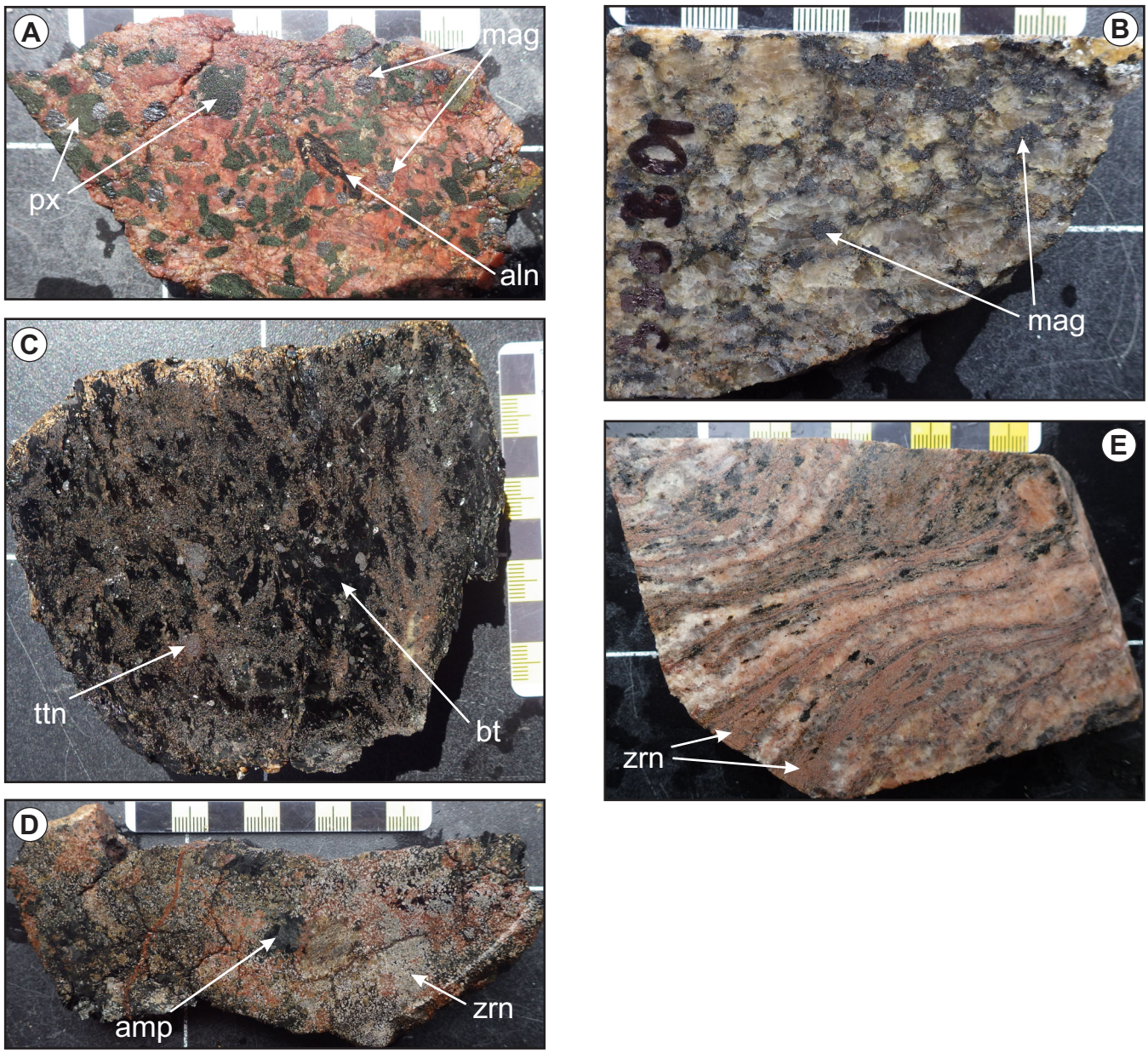

Plate 2. *Slabs of pegmatites. A) Magnetite- and pyroxene-rich pegmatite from Henley Harbour; B) Quartz- and magnetite-rich pegmatite from Southern Shore; C) Biotite- and titanite-rich pegmatite from HighREE; D) Zircon-rich pegmatite from Oceanview; E) Pegmatite with wisps of fine-grained zircon from HighREE. (Abbreviations* see *Whitney, 2010.)*

Table 1. List of REE and HFSE minerals occurring in the pegmatites

Mineral	Formula	Mineral	Formula
Allanite	(Ca, REE) (Al_2 Fe^{2+}) (Si_3O_{11}) O (OH)	Euxenite	(Y, Ca, Ce, U, Th) (Nb, Ta, Ti)$_2$ O_6
Fergusonite	(Y, La, Ce) Nb O4	Britholite	(Y, Ca) SiO_4
Monazite	REE (PO_4)	Chevkinite?	(Ce, La, Ca, Th)$_4$ (Fe^{2+}, Mg)$_2$ (Ti,Fe_8^{3+})$_3$ Si_4O_{22}
Bastnaesite	(Ce, Nd, Y) (CO_3) F	Yttrialite	(Y, Th)$_2$ Si_2O_7
Parisite	Ca (Ce, La, Nd, REE)$_2$ (CO_3)$_3$ F_2	Betafite	(Ca, Na, U)$_2$ (Ti, Nb, Ta)$_2$ O_6 (OH)
Synchisite	Ca (Ce, Nd, Y, REE) (CO_3)$_2$ F	Thorite	(Th,U) SiO_4

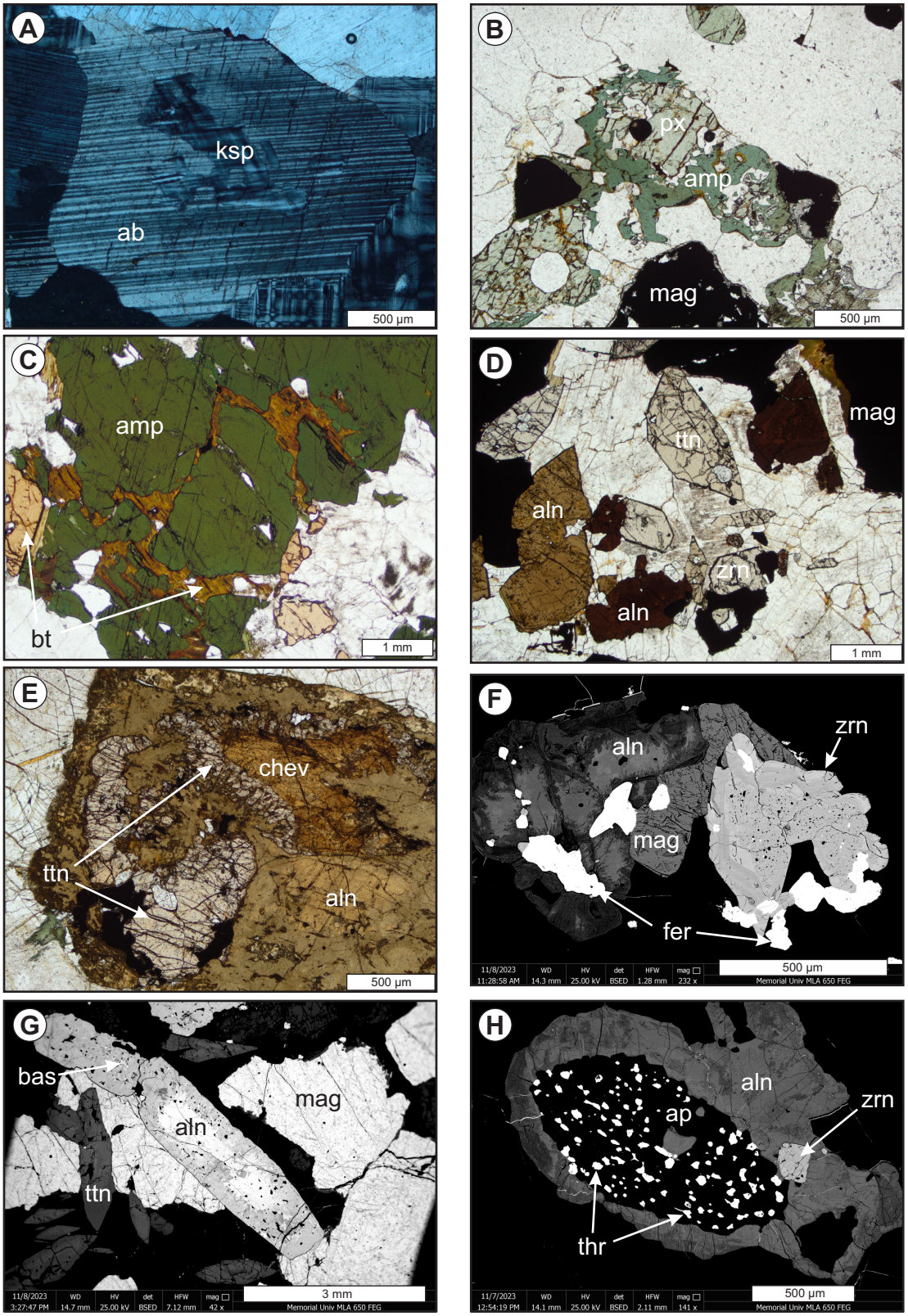

Plate 3. *Representative photomicrographs and back-scattered electron (BSE) images of minerals in the pegmatites. A) K-feldspar almost entirely replaced by albite from Oceanview; B) Pyroxene surrounded by amphibole from HighREE; C) Amphibole partially altered to biotite from Pesky Hill; D) Allanite with titanite, magnetite and zircon from Henley Harbour; E) Titanite partially replaced by allanite and a chevkinite-like mineral from HighREE; F) Zoned allanite with fergusonite and zoned zircon from Pesky Hill; G) Zoned allanite with bastnaesite in the rim from Henley Harbour; H) Apatite and thorite surrounded by allanite from Oceanview. (Abbreviations* see *Whitney, 2010.)*

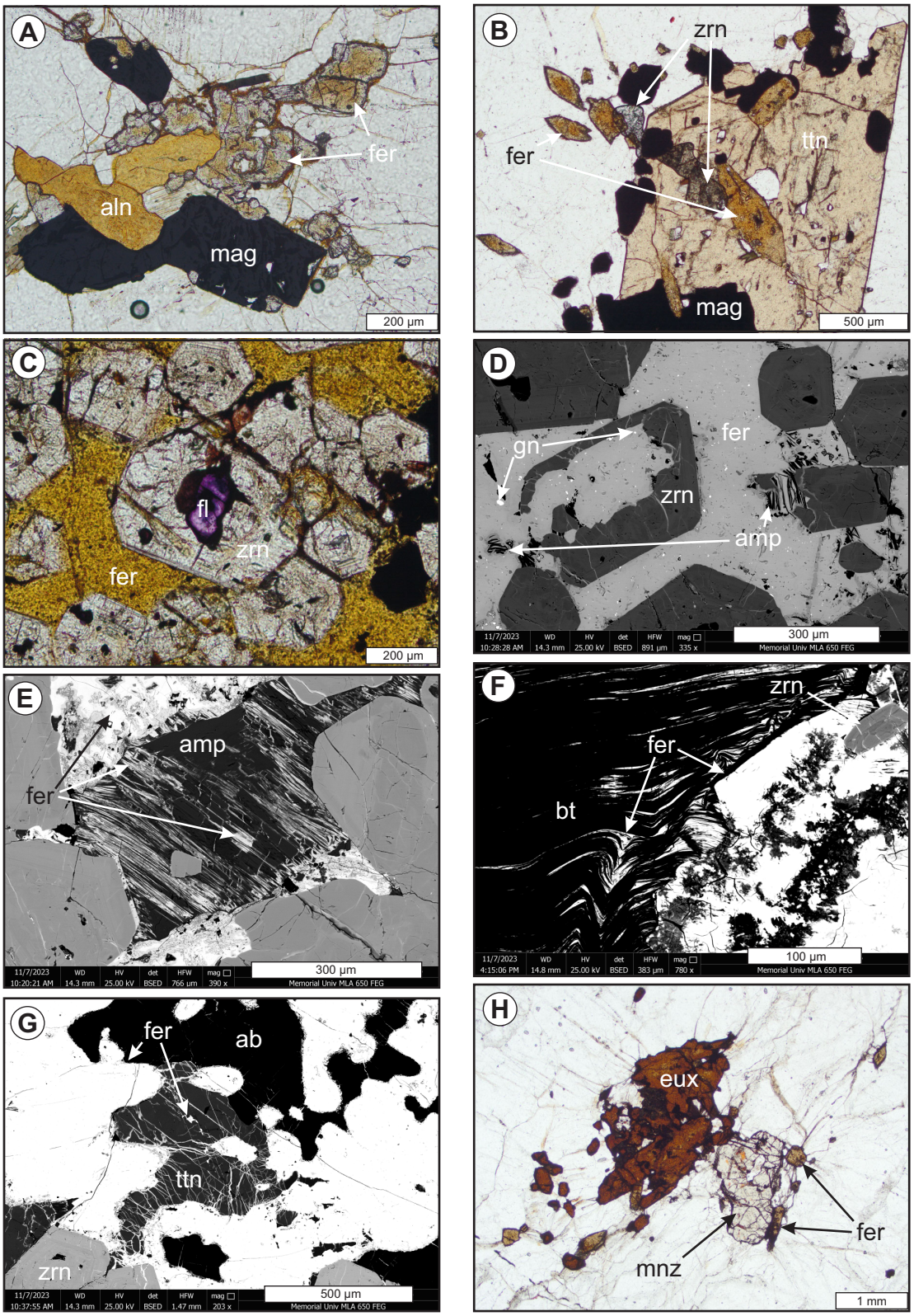

Plate 4. *Representative photomicrographs and back-scattered electron (BSE) images of minerals in the pegmatites. A) Fergusonite surrounding allanite from Pesky Hill; B) Fergusonite with titanite, magnetite and zircon from Southern Shore; C) Zircon containing inclusion of fluorite and surrounded by fergusonite from Oceanview; D) Fergusonite with inclusions of galena replacing zircon from Oceanview; E) Fergusonite replacing amphibole from Oceanview; F) Fergusonite replacing biotite from Oceanview; G) Fergusonite replacing titanite from Oceanview; H) Monazite with euxenite and fergusonite from Long Point. (Abbreviations* see *Whitney, 2010.)*

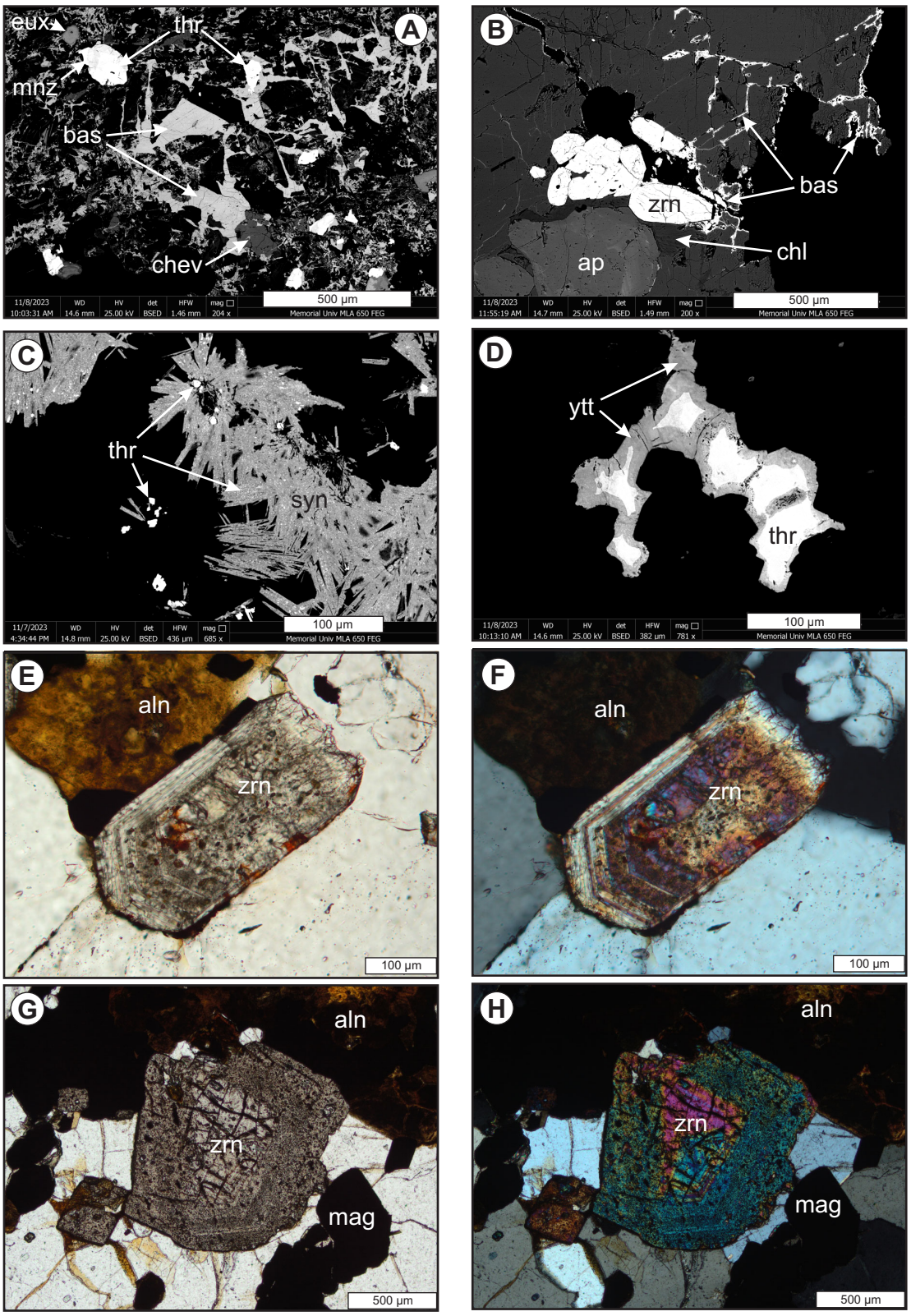

Plate 5. *Representative photomicrographs and back-scattered electron (BSE) images of minerals in the pegmatites. A) Monazite surrounding thorite occurring with euxenite, bastnaesite and a chevkinite-like mineral from Long Point; B) Bastnaesite replacing amphibole occurring with zircon and apatite from Toots Cove; C) Synchisite with thorite from Oceanview; D) Thorite surrounded by yttrialite from Long Point; E) Zoned zircon with inclusion-rich core and inclusion-free rim from HighREE; F) Same as E in cross-polarized light; G) Zoned zircon with inclusion-rich rim and inclusion-free core from HighREE; H) Same as G in cross-polarized light. (Abbreviations* see *Whitney, 2010.)*

and thorite (Plate 5A). Locally, yttrialite occurs surrounding thorite (Plate 5D).

High-field-strength-element (HFSE) minerals include zircon, thorite and betafite, from most to least common. Zircon is locally abundant and occurs in all areas. It is typically zoned with inclusion-rich cores and thin, inclusion-free rims (Plates 3F, 4C and 5E, F), although the opposite relationship has also been observed in a few samples (Plate 5G, H). The inclusions include REE minerals (*e.g.*, synchisite, bastnaesite and fergusonite), thorite and fluorite (Plate 4C). In samples containing wisps of fine-grained zircons at HighREE, the zircons are generally less than 30 µm in length and replace earlier minerals, such as amphibole (Plate 6A). Thorite is common, occurring in all areas and typically associated with REE minerals (Plate 5A, C, D), zircon, apatite (Plate 3H), and magnetite (Plate 6B). It is locally zoned. Betafite was only observed in one pegmatite at Oceanview, where it is abundant, and forms zoned euhedral crystals up to 2 mm in diameter (Plate 6C).

Volatile-rich minerals include apatite, fluorite and calcite. Apatite occurs in most pegmatites, commonly associated with allanite (Plate 3H) and other REE minerals. Fluorite is also very common forming late veins with calcite (Plate 6D), occurring as inclusions in zircon and enveloping zircons (Plate 4C) or along the cleavage planes of biotite. Calcite was only observed at Oceanview, where it is locally abundant replacing earlier minerals, such as amphibole (Plate 6E) and containing inclusions of REE minerals including allanite (Plate 6F).

Parent Intrusions

Most of the pegmatites are hosted in their parent intrusions, except for of a few that are hosted in older rocks. The parent intrusions range from granite to quartz-syenite and are composed of quartz, K-feldspar, albite, amphibole, pyroxene, biotite, magnetite, titanite, zircon, allanite, ilmenite, apatite, fluorite and calcite. Alteration ranges from weak to strong with pyroxene partially replaced by amphibole, amphibole partially replaced by biotite and/or chlorite, biotite altered to chlorite, K-feldspar is commonly albitized, allanite partially replaces amphibole, biotite, pyroxene and titanite, and magnetite is altered to hematite. Similar to the pegmatites, most zircon is zoned with inclusion-rich cores and inclusion-free rims.

GEOCHRONOLOGY

Six samples of pegmatites and their host intrusions from five of the areas were selected for geochronology to constrain the igneous crystallization ages of the rocks. They include two granites from HighREE (21ZM141A01 and 22ZM0427A01), one granite from Oceanview (22ZM0370A01), one pegmatite from Pesky Hill (22ZM0337C01), one granite from Henley Harbour (22ZM387A01), and one pegmatite from Long Point (22ZM0349A01; Plate 7). The results of the geochronology are summarized in Table 2. The igneous crystallization ages range from 1169 ± 11 and 1648.7 ± 4.8 Ma. All samples record zircon growth around 1000 Ma during Grenville orogeny.

Sample 21ZM141A01 (GSC Lab Number 12708)

The sample is a light-pink, foliated, medium-grained granite from HighREE hosting some of the REE pegmatites at that location (Plate 7A). It consists of quartz, K-feldspar, albite, amphibole, biotite, titanite and trace amounts of ilmenite, zircon and apatite.

An abundant zircon separate was collected directly from the Wilfley table (water shaking) consisting of clear,

Table 2. Summary of the results of the geochronology analyses

Sample Number	Lab Number	Area	Lithology	Age (Ma)	Interpretation
21ZM141A01	12708	HighREE	Granite	1648.7 ± 4.8	Igneous crystallization
21ZM141A01	12708	HighREE	Granite	*ca.* 1005–950	Metamorphism/partial melting
22ZM0427A01	12819	HighREE	Granite	1027.1 ± 8.2	Metamorphism/partial melting
22ZM0427A01	12819	HighREE	Granite	986 ± 15	Metamorphism
22ZM0370A01	12821	Oceanview	Syenite	1311 ± 12	Igneous crystallization
22ZM0370A01	12821	Oceanview	Syenite	1018 ± 11	Metamorphism
22ZM0337C01	12826	Pesky Hill	Pegmatite	*ca.* 1260	Igneous crystallization
22ZM0337C01	12826	Pesky Hill	Pegmatite	1019.7 ± 8.2	Metamorphism
22ZM0387A01	12820	Henley Harbour	Granite	1310 ± 12	Igneous crystallization
22ZM0387A01	12820	Henley Harbour	Granite	1024.1 ± 8.2	Metamorphism/partial melting
22ZM0349A01	12825	Long Point	Pegmatite	1500–2800	Inheritance
22ZM0349A01	12825	Long Point	Pegmatite	1169 ± 11	Maximum age of crystallization
22ZM0349A01	12825	Long Point	Pegmatite	1026 ± 11	Metamorphism

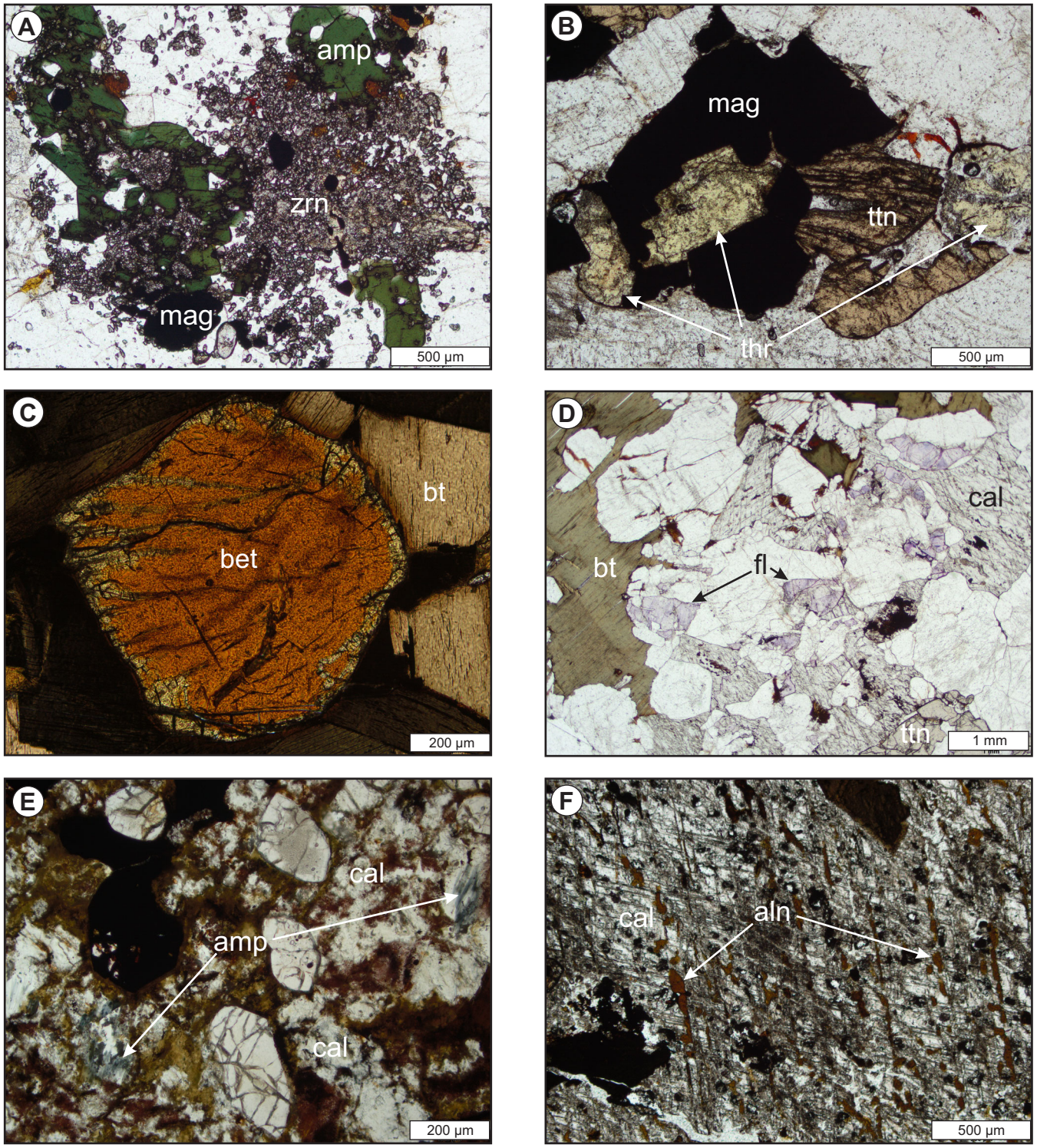

Plate 6. *Representative photomicrographs and back-scattered electron (BSE) images of minerals in the pegmatites. A) Fine-grained zircon replacing amphibole from HighREE; B) Thorite with magnetite and titanite from Piperstock Hill; C) Betafite from Oceanview; D) Abundant late fluorite and calcite from Oceanview; E) Calcite replacing amphibole from Oceanview; F) Calcite with inclusions of REE minerals including allanite from Oceanview. (Abbreviations* see *Whitney, 2010.)*

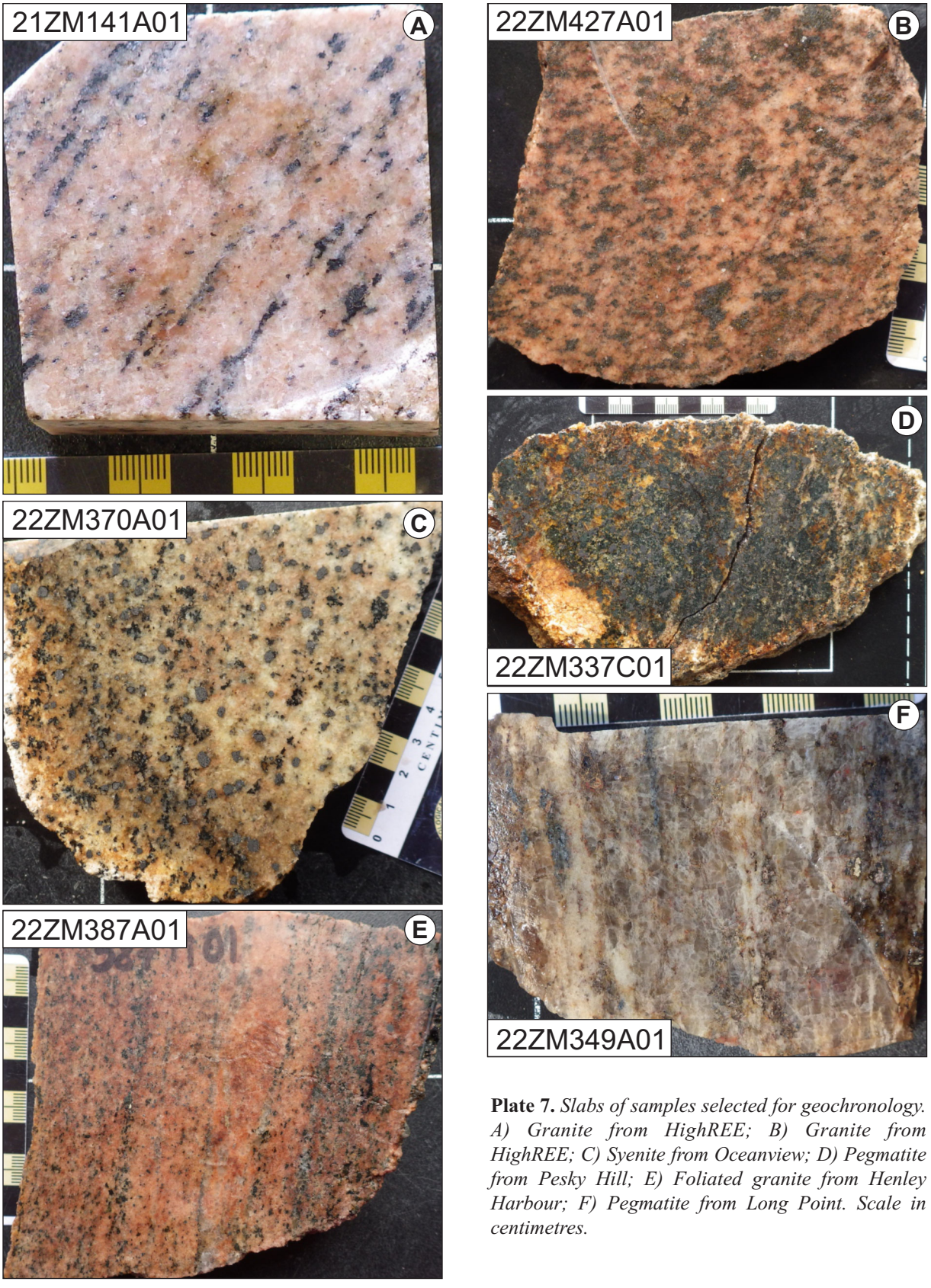

Plate 7. *Slabs of samples selected for geochronology. A) Granite from HighREE; B) Granite from HighREE; C) Syenite from Oceanview; D) Pegmatite from Pesky Hill; E) Foliated granite from Henley Harbour; F) Pegmatite from Long Point. Scale in centimetres.*

colourless prismatic grains (aspect ratio generally 2:1, 3:1). In CL, these are characterized by poor cathodoluminescence (CL) response (relatively high U) showing faint, broad sector and/or concentric zones (Figure 2A). In some cases, grains have a distinct "core/rim" relationship that strongly suggests a second generation of zircon growth (*e.g.*, grain 28, Figure 2A), whereas in other instances a broad "outer zone" might be a second growth domain or simply an extension of the zoning in the inner part of the grain (*e.g.*, grain 25, Figure 2A).

Thirty-two SHRIMP analyses were carried out on 28 separate zircon grains. Most of them form a single statistical population with a weighted mean $^{207}Pb/^{206}Pb$ age of 1648.7 ± 4.8 Ma (MSWD = 1.06, probability of fit = 0.39, Figure 2B). These analyses are from broad concentric or sector zones in both the inner and outer parts of grains. All have Th/U between 0.3 and 0.6. The remaining nine analyses are from distinct rims. Their high U content (1079–2689 ppm) suppresses their CL response making interpretation of the zoning difficult but some appear to be concentrically zoned. The rim analyses form a discordia chord with intercepts at 1004 ± 120 and 403 ± 260 Ma (MSWD = 2.1, Figure 2B). One analysis falls off the chord and is excluded from this regression as it might be nicking the core of the grain. The upper intercept is interpreted as the age of metamorphism. However, the concentric/oscillatory zoning is more consistent with igneous crystallization, suggesting the possibility of partial melting because of metamorphism. The oldest $^{206}Pb/^{238}U$ age for these rims (947 ± 22 Ma, 2s) could be considered a minimum age for this metamorphic/partial melting event. The significance of the lower intercept is unknown.

Although this granite hosts some of the pegmatites, it is interpreted as not a parent intrusion of the pegmatites, because it contains less LREE, Zr and Fe than most of the parent intrusion and a slightly smaller Eu anomaly, indicating that it is less evolved.

Sample 22ZM0427A01 (GSC Lab Number 12819)

The sample is a medium-pink, fine- to medium-grained weakly deformed granite from HighREE consisting of quartz, K-feldspar, albite, pyroxene, biotite and magnetite and trace amounts of ilmenite, hematite, zircon, and allanite (Plate 7B). It is altered and weathered with hematite replacing biotite, magnetite, and ilmenite.

An abundant zircon separate was recovered from the non-magnetic split (non-mag@1° side slope, 1,8A) using a Frantz isodynamic separator. The zircon grains consist of clear, colourless prismatic grains (aspect ratio generally 2:1, 3:1). In plane light, some grains have a high density of inclusions forming an inner cloudy "core", and many are fractured. In CL, the clear colourless zircons are characterized by a combination of oscillatory and sector zoning (Figure 2C). Some grains, though featureless in plane light, have discordant "contacts" between zoning styles that suggest the presence of both a core and a rim although this is ambiguous in most cases (*e.g.*, grain 35, 36, Figure 2C). The inner parts of the grains that are characterized by a high density of inclusions have very convolute/chaotic zoning (*e.g.*, grain 33, 34, Figure 2C).

Thirty-four SHRIMP analyses were carried out on 22 separate zircon grains. Analyses of both convolute cores and oscillatory zoned "rims" yield a single statistical population with a weighted mean $^{206}Pb/^{238}U$ age of 1027.1 ± 5.1 Ma (± 8.2 Ma long-term reproducibility, n=24, MSWD = 1.3, probability of fit 0.16, Figure 2D). This excludes two slightly older as well as 8 analyses of rims that yield distinctly younger ages. These rims are very similar in appearance and chemistry to those forming part of the 1027 Ma population; however, they give consistently younger ages with a weighted mean $^{206}Pb/^{238}U$ age of 986 ± 15 Ma (n=7, MSWD = 2.6, probability = 0.017, Figure 2D). Given the oscillatory zoning observed in both populations, it is inferred that anatectic, rather than solid-state processes are at work during these metamorphic events. However, the geological significance of these events and any possible links to mineralization are unknown.

It is notable that despite the clear presence of inclusion-rich or chaotically zoned cores and oscillatory-zoned rims, there is no discernable age difference between them and there is no evidence of a *ca.* 1.3 Ga event in this granite. However, due to the similarities in mineralogy (abundant magnetite, zircon, titanite and allanite) and chemistry of this granite to other parent intrusions (A-type, metaluminous, within-plate granite; *see* the Geochemistry section below) and the REE pegmatites, it is interpreted to be one of the parent intrusions of the pegmatites. A pantellerite sample from Deep Fox displays similar features with inclusion-rich zircon cores and gave metamorphic ages, except for one core yielding 1238 Ma (Magyarosi and Rayner, 2023).

Sample 22ZM0370A01 (GSC Lab Number 12821)

The sample is a light-pinkish beige, medium-grained, undeformed syenite from Oceanview consisting of K-feldspar, albite, quartz, magnetite, amphibole, biotite and titanite and trace amounts of apatite, ilmenite, zircon, calcite and allanite (Plate 7C).

An abundant zircon separate was recovered directly from the Wilfley table, no further mineral separation steps were carried out prior to hand picking. The zircon grains consist of clear, colourless prismatic to ovoid grains (aspect

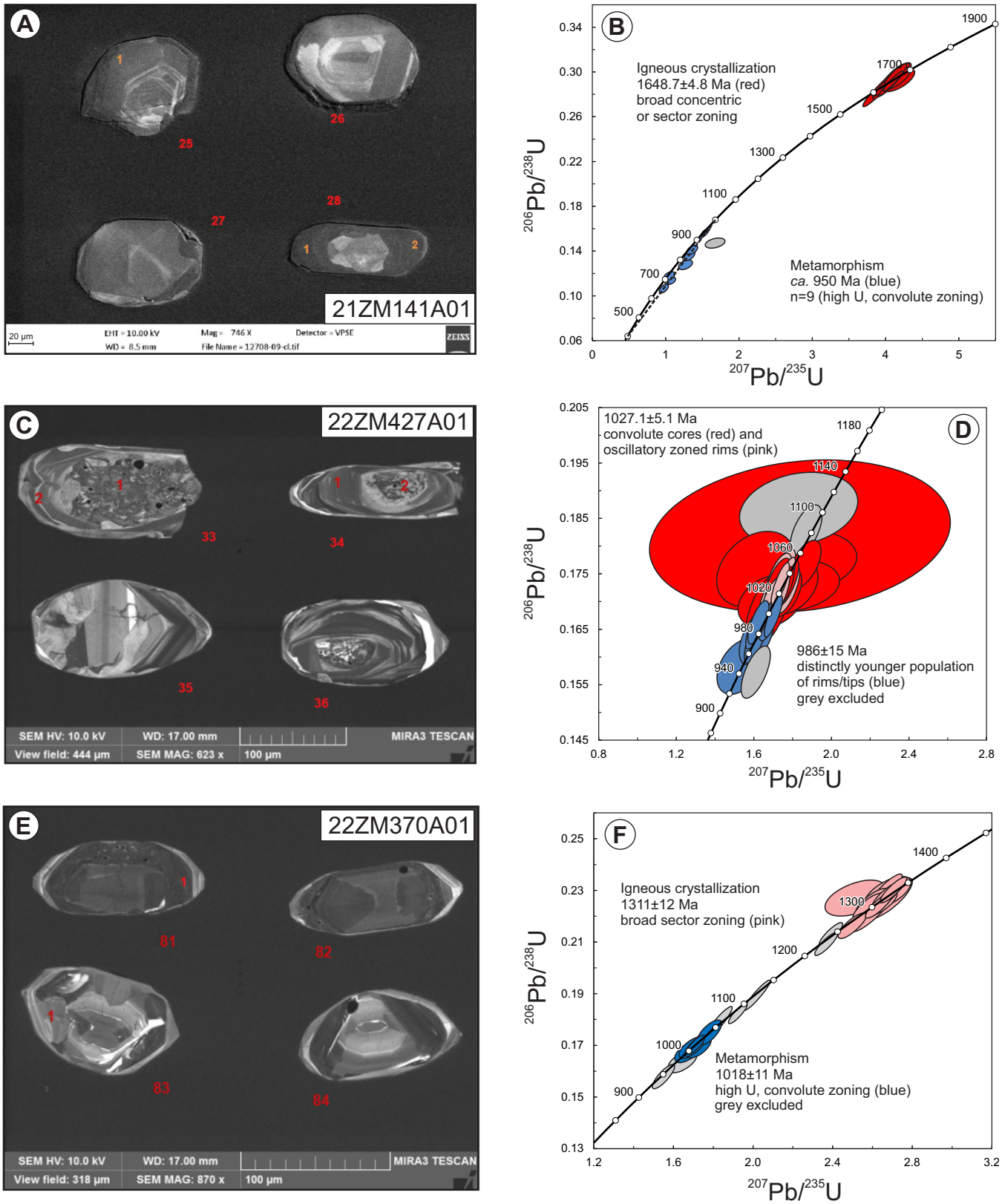

Figure 2. *Cathodoluminescence (CL) images of zircons and concordia diagrams of the geochronology samples. A, B) Granite from HighREE; C, D) Granite from HighREE; E, F) Syenite from Oceanview.*

ratio generally 2:1, 3:1). Core/rim relationships are not apparent in plane light. In CL, the zircons are characterized by cores with broad, sector zonation surrounded by rims (*e.g.*, grains 81, 82, Figure 2E). The zoning in the rims is variable, some exhibit finer concentric zoning, others are more chaotic, while yet others appear unzoned (Figure 2E).

Thirty SHRIMP analyses were carried out on 28 separate zircon grains. The 14 oldest analyses are all from zircons with broad, sector zoning and yield a weighted mean $^{206}Pb/^{238}U$ age of 1311 ± 12 Ma (MSWD = 2.7, probability of fit = 0.001, Figure 2F), which is interpreted as the igneous crystallization age. Analysis of 16 rims yield a range of ages from 1245 to 945 Ma. Most of them cluster at *ca.* 1.0 Ga, with nine of them yielding a weighted mean $^{206}Pb/^{238}U$ age of 1018 ± 11 Ma (MSWD = 2.4, probability of fit = 0.013, Figure 2F) and is interpreted as a metamorphic overprint. The remainder are spread along concordia up to the cluster at *ca.* 1.3 Ga and likely represent incomplete resetting/recrystallization of the older 1.3 Ga component.

Sample 22ZM0337C01 (GSC Lab Number 12826)

The sample is a light to dark grey, medium-grained, weakly deformed pegmatite from Pesky Hill consisting of albite, pyroxene, magnetite, titanite, REE-minerals and trace amounts of quartz, amphibole, apatite, zircon, and ilmenite (Plate 7D).

An abundant zircon separate was recovered from the non-magnetic split (non-mag@1° side slope, 1,8A) using a Frantz isodynamic separator. The zircon grains consist of clear, colourless prismatic to ovoid grains (aspect ratios generally 2:1, 3:1). Core/rim relationships are not apparent in plane light. In CL, many of the grains are either entirely composed of, or have inner portions with, blocky/sector zoning where the individual sectors may exhibit fine lamellar zoning (*e.g.*, grain 1, Figure 3A). In other instances, the cores/grains are unzoned or faintly zoned (*e.g.*, grain 2, Figure 3A). Where cores are apparent, these are surrounded by rims that exhibit irregular or concentric zoning or may be unzoned (*e.g.*, grains 3, 4, Figure 3A). This same style of zoning is also observed in discrete grains, not just rims.

Thirty-six SHRIMP analyses from 30 zircon grains yield two groups of ages. The blocky/sector/lamellar zoned zircons form a cluster of ages around 1260 Ma. The weighted mean $^{206}Pb/^{238}U$ age of the oldest 13 analyses is 1262 ± 10 Ma (MSWD = 2.2, probability = 0.008, Figure 3B). The rims, as well as the unzoned, concentrically zoned or irregularly zoned zircons, yield a weighted mean $^{206}Pb/^{238}U$ age of 1019.7 ± 5.3 Ma (± 8.2 Ma long-term reproducibility, n=18, MSWD = 1.4, probability = 0.13, Figure 3B). The igneous crystallization age of this rock is interpreted to be 1262 ± 10 Ma and the spread of ages down to as young as 1220 Ma is attributed to Pb-loss from a 1019.7 ± 8.2 Ma metamorphic event.

Sample 22ZM0387A01 (GSC Lab Number 12820)

The sample is a dark-pink, foliated, medium-grained granite from Henley Harbour consisting of K-feldspar, quartz, albite, pyroxene, magnetite, titanite and trace amounts of amphibole, zircon, allanite, apatite, hematite, and fluorite (Plate 7E).

An abundant zircon separate was recovered from the non-magnetic split (non-mag@1° side slope, 1,8A) using a Frantz isodynamic separator. The zircon grains consist of two morphologies: one is sharply faceted, clear, colourless, and prismatic with no inclusions or fractures, while the other is rounded/ovoid, pale brown, and commonly contains large inclusions. In thin section, some of the inclusions in zircon were identified as fluorite, similar to the Oceanview parent intrusions and pegmatites. In CL, the sharply faceted grains exhibit concentric zoning (*e.g.*, grain 99, Figure 3C). The pale-brown ovoid grains commonly exhibit chaotic zoning, and, in some instances, a chaotically zoned core is surrounded by a sharply terminated, regularly zoned rim (*e.g.*, grain 97, 98, Figure 3C).

Thirty-two SHRIMP analyses were conducted on 27 individual zircon grains. The results cluster in two groups, largely consistent with their morphology and zoning. The chaotically zoned zircon and cores cluster with a weighted mean $^{206}Pb/^{238}U$ age of 1310 ± 12 Ma (n=12, MSWD = 1.5, probability of fit = 0.11, Figure 3D), interpreted as the crystallization age of the granite. A younger cluster with a weighted mean $^{206}Pb/^{238}U$ age of 1024.1 ± 7.0 Ma (± 8.2 Ma long-term reproducibility, n=16, MSWD = 1.3, probability of fit = 0.20, Figure 3D) consists primarily of concentrically zoned zircons as well as rare ambiguously zoned zircon. Three analyses are intermediate between these two end-members and are interpreted as recording incomplete resetting of the 1310 Ma zircon by the event responsible for zircon growth at 1024 Ma. Similar to samples 21ZM141A01, 22ZM427A01 and 22ZM370A01, the oscillatory zoning in the younger zircon population is more characteristic of igneous zircon and indicates partial melting during metamorphism.

Sample 22ZM0349A01 (GSC Lab Number 12825)

The sample is a foliated, light-brownish-grey, medium- to coarse-grained pegmatite from Long Point consisting of quartz, K-feldspar, albite, hematite, zircon, REE minerals and trace amounts of titanite, magnetite, calcite, ilmenite, thorite and muscovite (Plate 7F). The REE minerals include

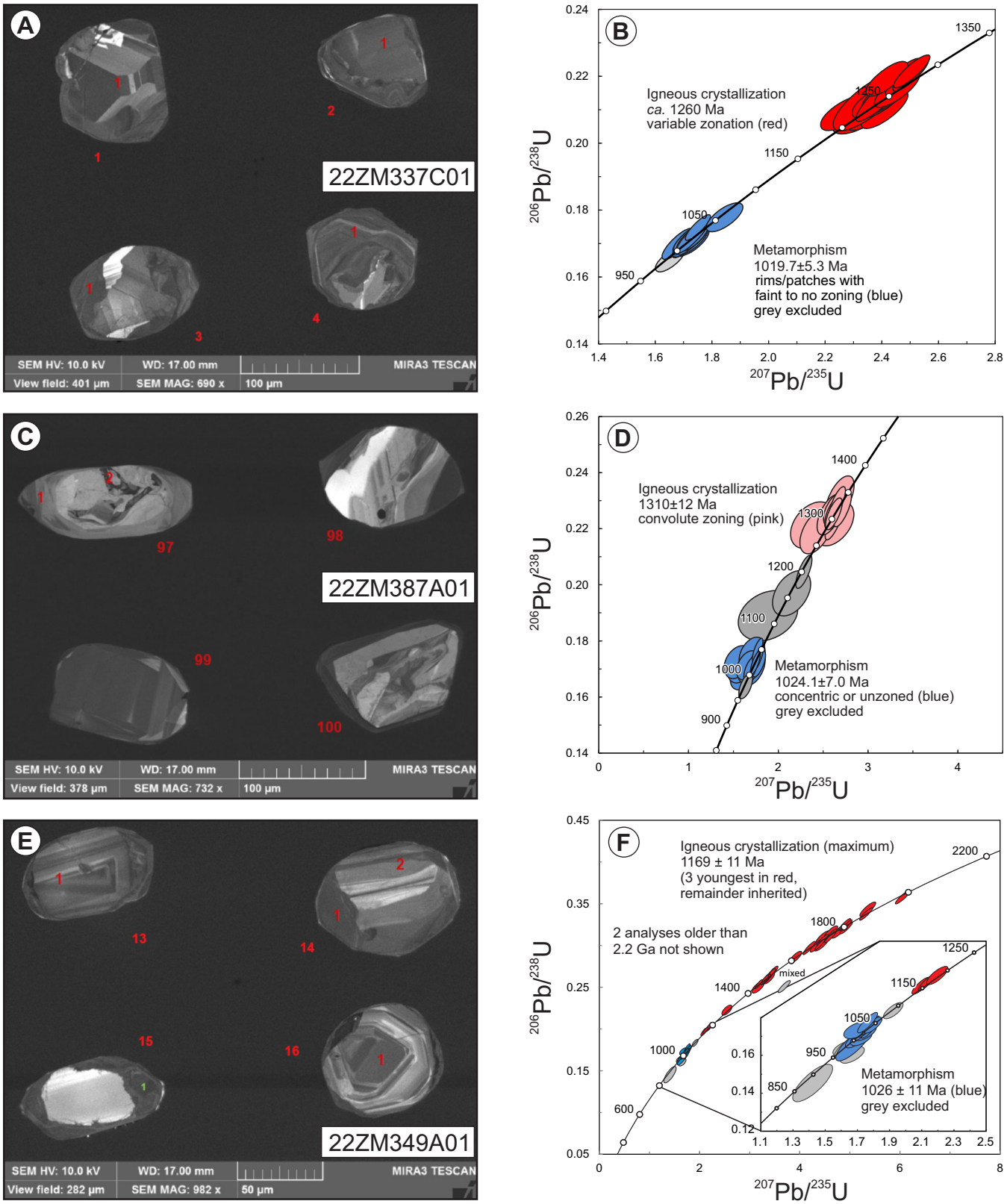

Figure 3. *Cathodoluminescence (CL) images of zircons and concordia diagrams of the geochronology samples. A, B) Pegmatite from Pesky Hill; C, D) Granite from Henley Harbour; E, F) Pegmatite from Long Point.*

allanite, fergusonite, bastnaesite, monazite, euxenite, yttrialite and a chevkinite-like mineral.

An abundant zircon separate was recovered from the non-magnetic split (non-mag@3° side slope, 1,8A) using a Frantz isodynamic separator. The zircon grains consist of prismatic to ovoid grains (aspect ratio generally 2:1, 3:1) that are variably clear and colourless to pale brown and cloudy. Core/rim relationships are not apparent in plane light. In CL images, the grains are characterized by discrete grains or cores with well-developed, fine-scale oscillatory (*e.g.*, grains 13, 14, 16, Figure 3E) or convolute zoning. Most of these grains are surrounded by CL-dark (high U), unzoned, or faintly zoned rims (*e.g.*, grains 14, 15, Figure 3E).

Fifty-two analyses were carried out on 47 individual zircon grains. The oscillatory and convolutely zoned grains/cores yield a wide range of ages from 1157 to 2822 Ma with clusters at 1500 and 1700–1800 Ma (Figure 3F). The youngest cluster of reproducible ages from this population consists of 3 grains with a weighted mean $^{206}Pb/^{238}U$ age of 1169 ± 11 Ma (2s; ± 36 Ma 95% confidence MSWD = 2.1, probability of fit = 0.12). This age is considered the maximum crystallization age of this rock, with the older zircon grains representing inherited components. Dark unzoned rims yield a weighted mean $^{206}Pb/^{238}U$ age of 1026 ± 11 Ma (n=11, MSWD = 2.7, probability of fit = 0.002), which is interpreted as the age of metamorphism.

GEOCHEMISTRY

The parent intrusions range from granite to syenite (Figure 4A) and are mostly metaluminous (Figure 4B) and A-type (Figure 4C). The few samples outside of the granite and syenite fields are altered, affected by Na- or K-metasomatism (Figure 5A, B), although other elements were also clearly remobilized based on petrography. The Zr content ranges up to 21 800 ppm indicating that the host rocks are highly evolved (Figure 4C). With few exceptions, they fall

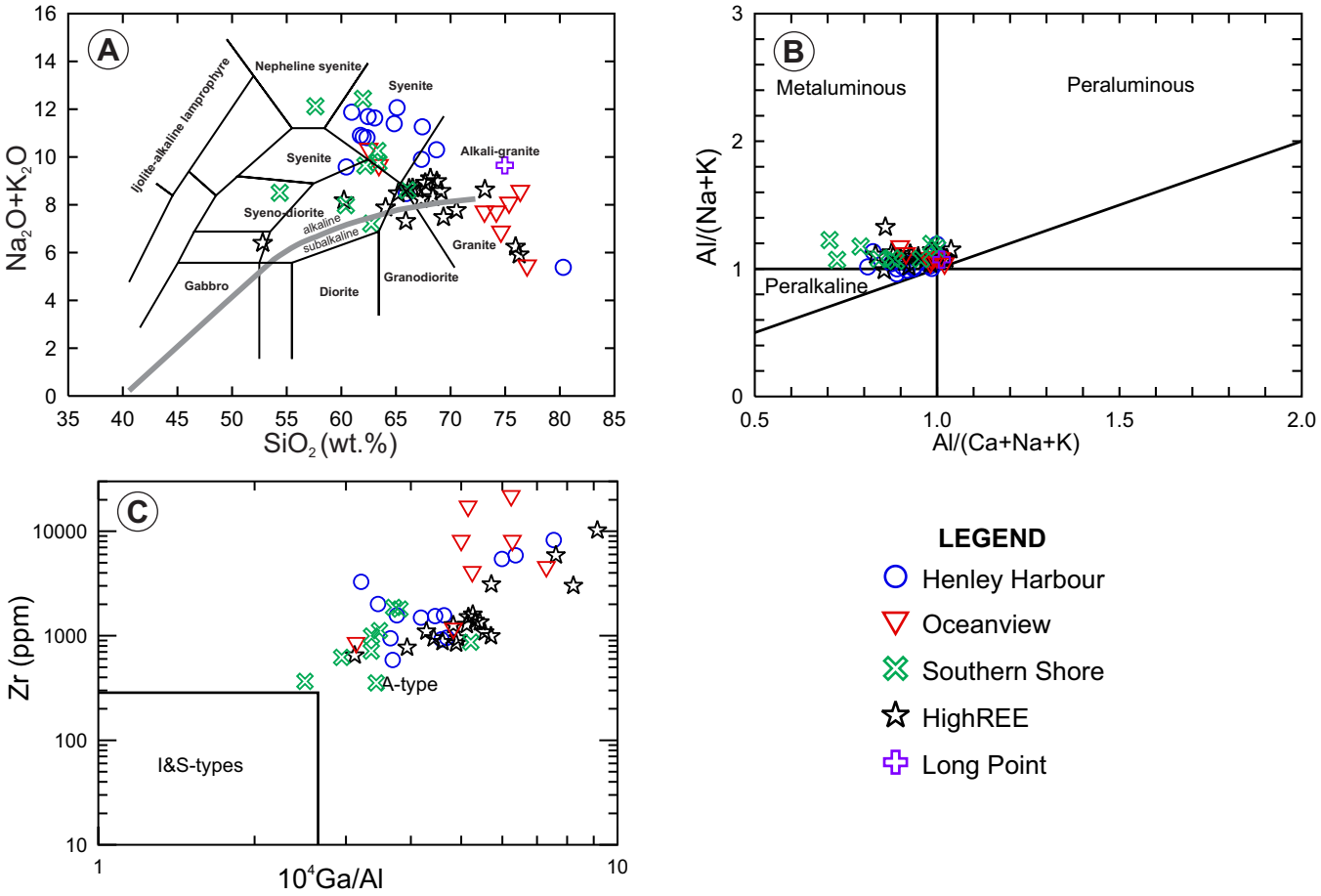

Figure 4. *Chemical classification of the parent intrusions. A) Total alkalies* vs. *SiO_2 plutonic rock classification (Wilson, 1989); B) Al/(Na+K) molar ratio* vs. *aluminum-saturation index (Shand, 1922); C) Zr* vs. *10^4Ga/Al (Whalen* et al.*, 1987). On all figures (4 to 7), Southern Shore includes the Southern Shore, Piperstock Hill, Pesky Hill and Toots Cove pegmatites and parent intrusions.*

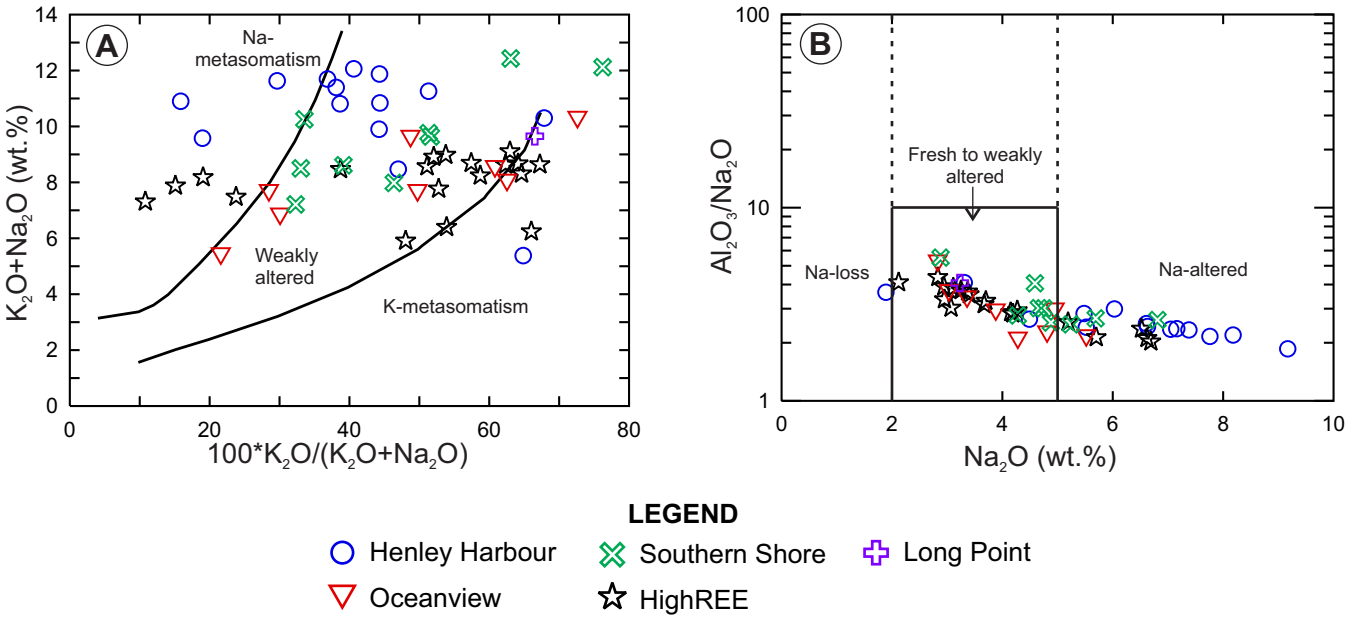

Figure 5. *Diagrams showing the effects of alteration and/or metamorphism. A) Hughes (1973) diagram separating weakly altered, and K- and Na-metasomatized rocks; B) Spitz and Darling (1978) diagram separating fresh to weakly altered rocks from rocks affected by Na loss or gain.*

in the within-plate granite (WPG) field (Figure 6) and are straddling the boundary between A1- and A2-types (Figure 7; Whalen and Hildebrand, 2019). A few samples from Oceanview fall in the ocean-ridge granite (ORG) field (Figure 6A, B), but the reason for this is alteration leading to relative enrichment in HREE and HFSE. These samples are strongly altered with amphibole and biotite almost entirely replaced by unidentified rusty brown minerals (allanite and other REE minerals).

On chondrite normalized REE plots, most of the parent intrusions display a negative slope from La to Lu and a negative Eu anomaly (Figure 8A). A few samples from Oceanview and all samples from Long Point display a flat REE pattern or a very weak positive slope from La to Lu. The extended trace-element plots show negative Ba, Sr, P and Ti anomalies and positive Th, U, Ta and Pb anomalies (Figure 8B). The chondrite normalized REE plots of the pegmatites are similar to the parent intrusions but show stronger enrichments in all REE, especially HREE, resulting in smaller negative slopes or weak positive slopes from La to Lu (Figures 8C and 9A, C, E, G, I). In the extended trace-element plots, the pegmatites show stronger positive and negative anomalies of the same elements than the parent intrusions, consistent with their more evolved nature (Figures 8C and 9B, D, F, H, J). The LREE enrichment in the parent intrusions is up to ~6000 times and the HREE enrichment is up to ~1000 times the chondrite values (Figure 8A). The LREE and HREE enrichment in the pegmatites is up to ~20 000 times the chondrite values (Figure 8C). These enrichments indicate that both parent intrusions and pegmatites are strongly fractionated, and the degree of fractionation is stronger in the pegmatites in every area. In addition, the pegmatites show a relatively stronger enrichment in HREE compared to the LREE than the parent intrusions.

The parent intrusions are geochemically similar to the FHVB (Magyarosi and Rayner, 2023). Felsic rocks in the FHVB range in composition from rhyolite to trachyte and are A-type, straddling the boundary between the A1- and A2-type, and fall in the WPG field. The FHVB felsic rocks are also mostly metaluminous, but there are more peralkaline samples compared to the parent intrusions to the south. Compared to the pantellerites in the FHVB, the parent intrusions in the study area appear to be slightly less enriched in both LREE and HREE, comparable to comendite and non-peralkaline rhyolite (Magyarosi and Rayner, 2023). The LREE enrichment in the pegmatites is similar to the pantellerites, but the pegmatites have smaller negative or weakly positive slopes, indicating their higher overall REE content, especially the HREE content, which is more than ~10 times the HREE content of pantellerites in the FHVB.

DISCUSSION

The various types of alteration observed in the pegmatites indicate that they were affected by more than one hydrothermal event followed by Grenvillian metamorphism. Several of these alteration types are present in the parent

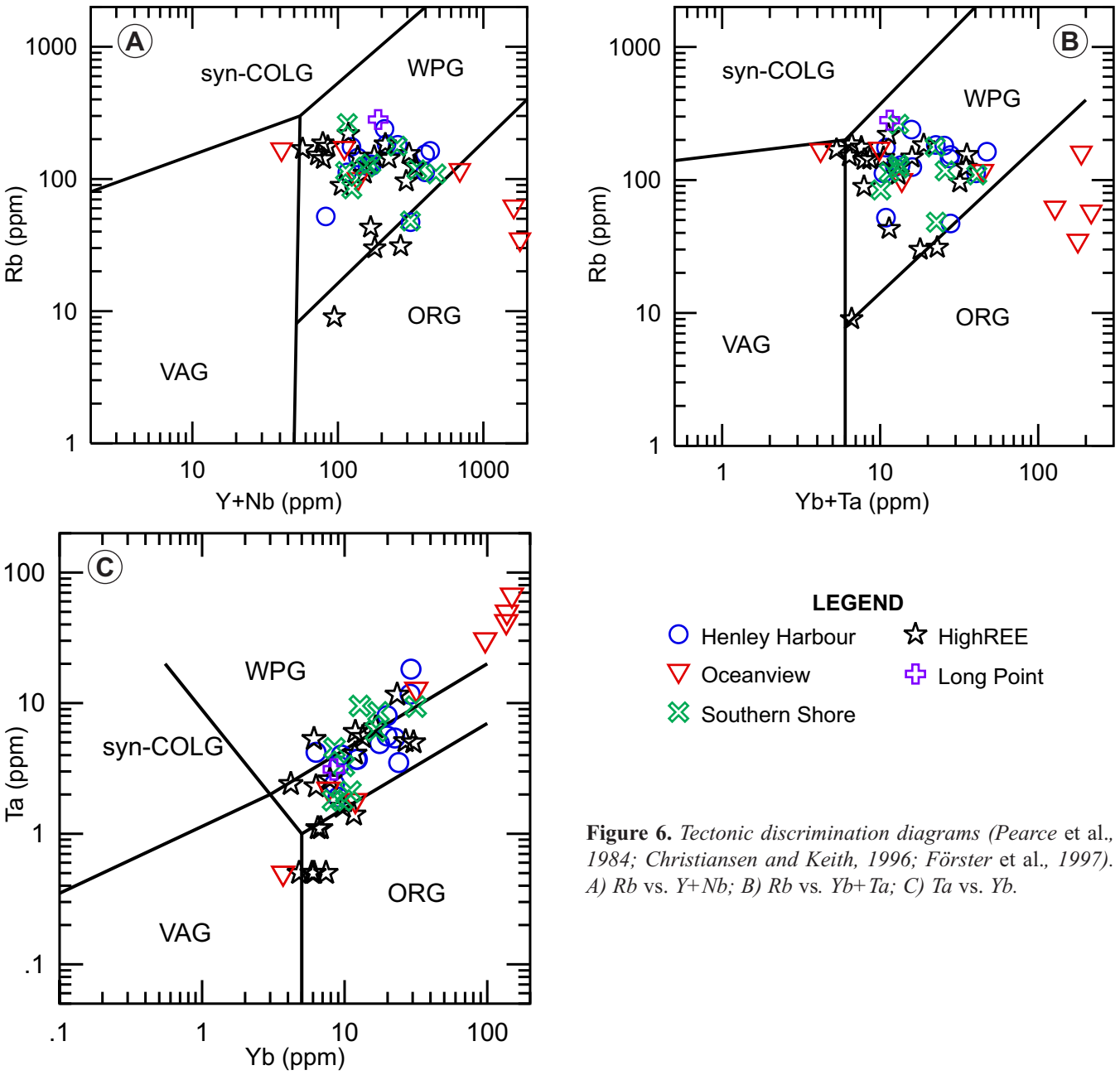

Figure 6. *Tectonic discrimination diagrams (Pearce* et al.*, 1984; Christiansen and Keith, 1996; Förster* et al.*, 1997). A) Rb* vs. *Y+Nb; B) Rb* vs. *Yb+Ta; C) Ta* vs. *Yb.*

intrusions as well, including albitization of K-feldspar, alteration of pyroxene to amphibole and amphibole to biotite, and allanite replacing amphibole, biotite and titanite; effects of which are observed in the geochemistry of the rocks (Figure 5). In the pegmatites, allanite and fergusonite are at least partially hydrothermal, with fergusonite locally crystallizing later than allanite, suggested by their textural relationships. Allanite, and other earlier minerals such as amphibole, pyroxene, biotite and thorite, are later replaced by REE-fluorocarbonates or monazite. The inclusion-rich nature of the core of the zircons suggest that the core of the zircons is most likely hydrothermal as well. The effect of metamorphism on the REE minerals is uncertain, but age data from inclusion-free and younger rims of zircon indicate new zircon growth during Grenville metamorphism (*ca.* 1030–950 Ma).

The best evidence for hydrothermal remobilization of REE and HFSE are the Oceanview pegmatites and their parent granite, which are the most enriched in these elements compared to the other pegmatites and parent intrusions, respectively, but are also the most volatile-rich and most strongly altered. They also show the most variability in the spider diagrams (Figure 9C). The core of zircons in the peg-

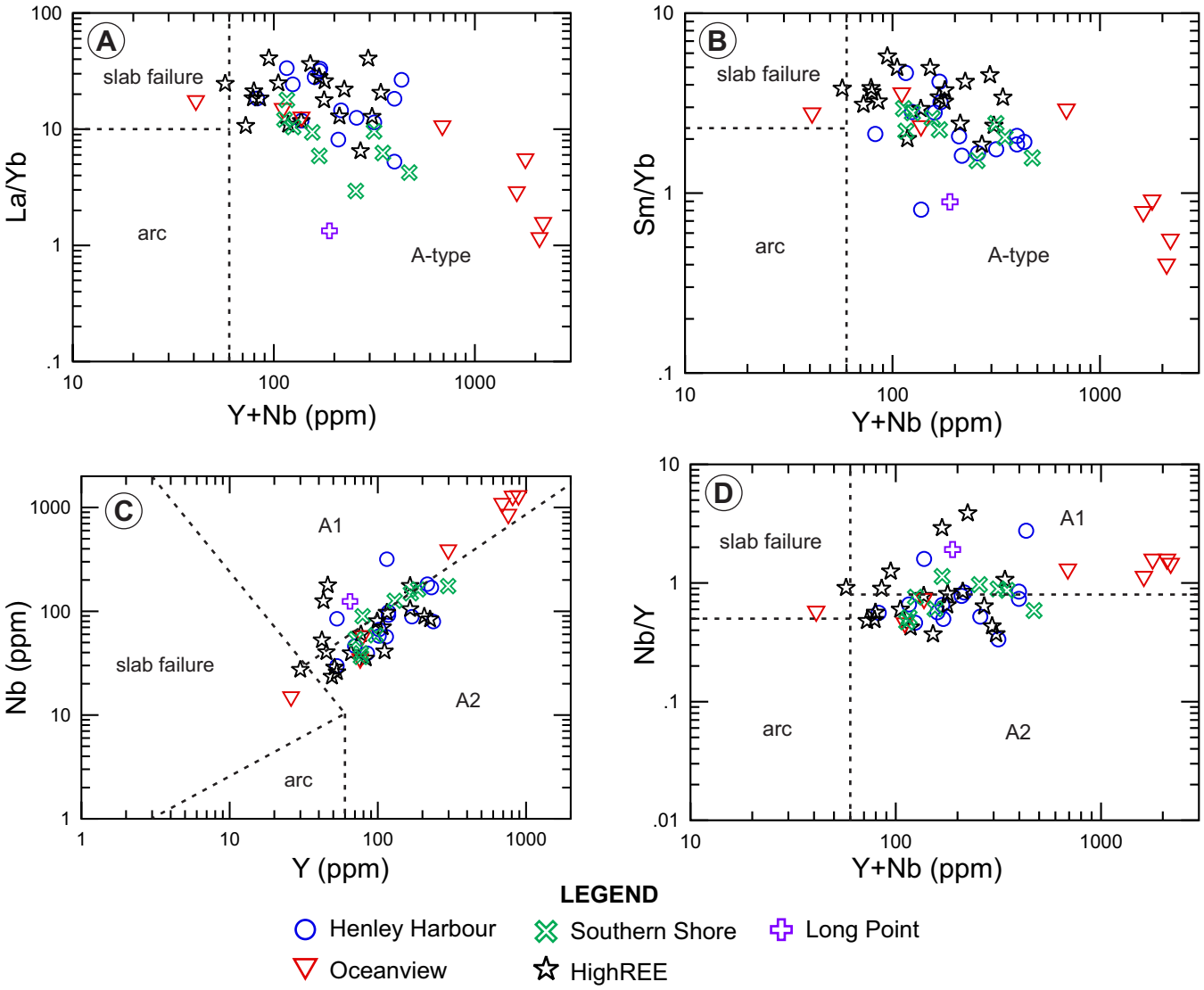

Figure 7. *Diagrams distinguishing the A, A1 and A2 granites (Whalen and Hildebrand, 2019). A) La/Yb* vs. *Y+Nb; B) Sm/Yb* vs. *Y+Nb; C) Nb* vs. *Y; D) Nb/Y* vs. *Y+Nb.*

matites contains abundant inclusions, including fluorite. The pegmatites from Oceanview also contain abundant fluorite and calcite (Plate 6D) replacing amphibole (Plate 6E), occurring in zircon (Plate 4C), or containing REE minerals (Plate 6F). This suggests that F- and C-rich volatiles played an important role in alteration and REE- and HFSE-enrichment in both the pegmatites and parent intrusions.

Hydrothermal alteration of REE pegmatites and parent intrusions leading to remobilization of REE and HFSE was studied in detail at Strange Lake (Vasyukova and Williams-Jones, 2018) and it was interpreted to be autometasomatic, attributed to volatiles exsolving from the cooling parent intrusion. At Strange Lake, LREE were remobilized at higher temperatures (~400°C) and HREE were remobilized at lower temperatures (~150°C) with the chemistry of the exsolved fluid changing as a result of cooling and interactions with the minerals in the cooling magma (Vasyukova and Williams-Jones, 2018). Evidence from this study suggest that similar magmatic and magmatic-hydrothermal processes were responsible for the REE and HFSE mineralization in the pegmatites and their parent intrusions south of the FHVB.

The parent intrusions and pegmatites show many similarities to the FHVB: 1) similar ages of igneous crystallization (~1269–1314 Ma; Magyarosi and Rayner, 2023); 2) similar wholerock geochemistry (A-type, WPG, metaluminous to peralkaline, granitic to syenitic, similar REE ranges); 3) same REE mineralogy (Magyarosi and Rayner, 2023); and 4) same silicate mineralogy and mineral chemistry, suggesting that some of the parent intrusions south of

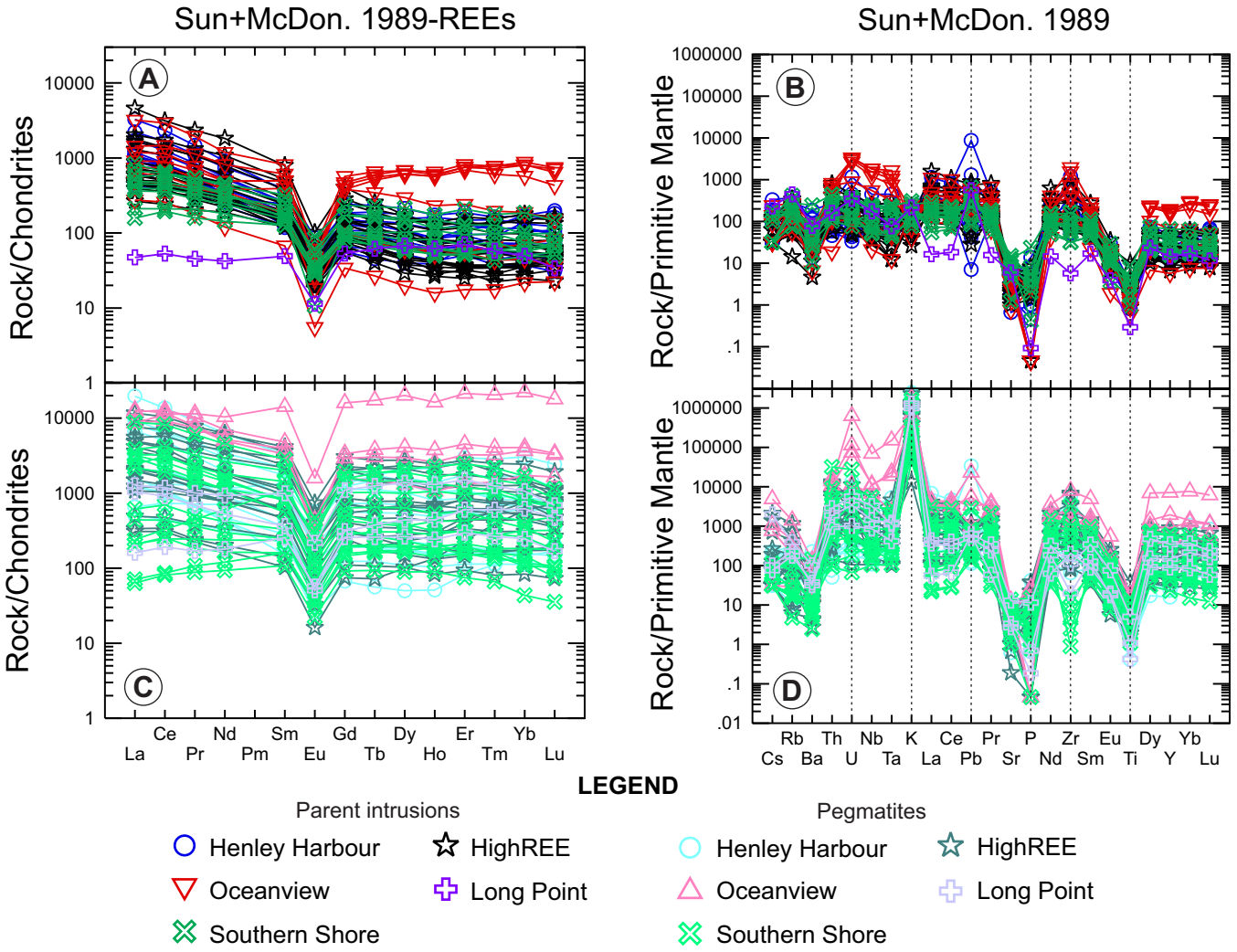

Figure 8. *Chondrite-normalized REE patterns and primitive mantle-normalized plots (Sun and McDonough, 1989). A, B) Parent intrusions; C, D) Pegmatites.*

the FHVB may potentially represent the intrusive equivalents of the FHVB. This is consistent with the presence of pegmatites in the intrusions and lack of them in the FHVB. The lack of more peralkaline rocks to the south may be due to the examined rocks occurring near the pegmatites and representing the top of these intrusions that are more likely to be autometasomatized by volatiles moving up within the intrusions. This study suggests that all rocks belonging to the ~1311–1260 Ma event in the Fox Harbour area may be genetically related.

CONCLUSIONS

Rare-earth element and HFSE mineralization in the pegmatites south of the FHVB are the result of magmatic and late-magmatic hydrothermal processes and may have been modified by later metamorphism. Late-magmatic processes were due to volatiles exsolving from the cooling parent intrusions of the pegmatites leading to alteration and remobilization of REE and HFSE.

Mineralogy, mineral chemistry, and geochronology of some of the pegmatites and parent intrusions are similar to those observed at the FHVB; suggesting that they may potentially represent the intrusive equivalents of the FHVB. Although the effects of Grenvillian metamorphism and deformation complicates the identification of the processes leading to REE and HFSE mineralization, the study area provides a unique opportunity to examine a peralkaline complex at depth, as most undeformed complexes are typically exposed only on top of the intrusions (*e.g.*, Flowers River, Strange Lake). More detailed studies are needed to understand the genesis of these rocks and the associated REE and HFSE mineralization.

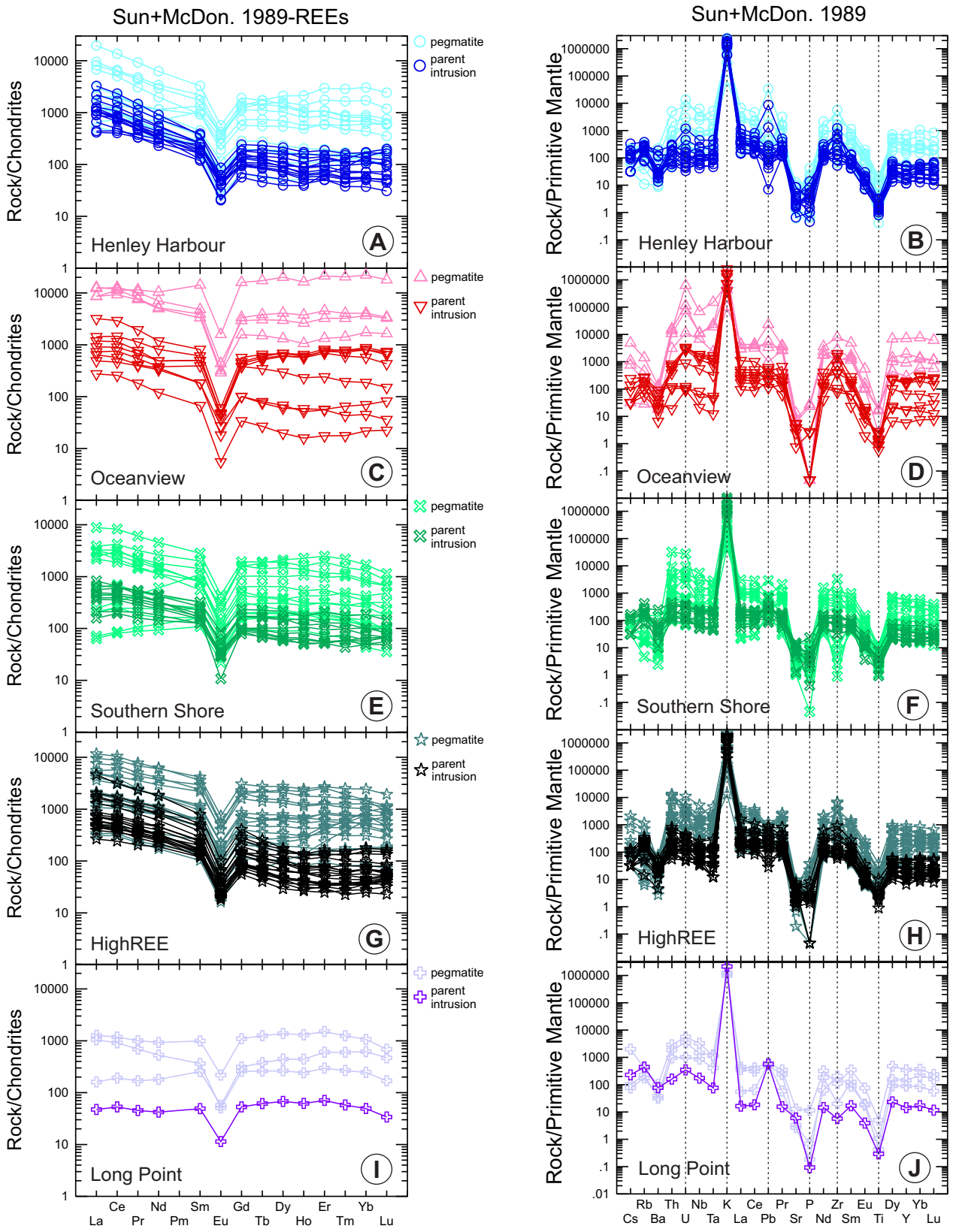

Figure 9. *Chondrite-normalized REE patterns and primitive mantle-normalized plots of pegmatites and their parent intrusions (Sun and McDonough, 1989). A, B) Henley Harbour; C, D) Oceanview; E, F) Southern Shore (Pesky Hill, Toots Cove, Southern Shore and Piperstock Hill); G, H) HighREE; I, J) Long Point.* See *legend on Figure 8.*

The area south of the FHVB is very prospective for additional REE and HFSE mineralization. Further exploration should include a combined airborne radiometric and magnetic survey to aid in identification of the various rock units. More detailed ground radiometric and magnetic surveys could aid in locating additional pegmatites; however, such surveys are limited as locating pegmatites that are not at surface may be difficult, because the radiometric survey penetrates only 30 cm and the host rocks, which are typically the parent intrusions, are also commonly magnetic.

ACKNOWLEDGMENTS

This paper is a contribution to Natural Resources Canada's (NRCan) TGI Program of the GSC. Support for this study was provided through the Magmatic Ore Systems Project's 'Sub-Activity: Critical minerals within carbonatite, syenite and allied peralkaline-alkaline rocks in the central and eastern parts of the Canadian Shield: where, when and how were they formed' and by the GSNL. Lindsay Oldham and Arianna Sheppard are thanked for their assistance during fieldwork in the summers of 2021 and 2022. Gerry Hickey helped with providing some of the equipment for and after the fieldwork. Joanne Rooney and Kim Morgan are acknowledged for typesetting and figure preparation, respectively. ZM is grateful to Randy Miller and the crew from Search Minerals Incorporated for their tremendous help during both field seasons. John Hinchey (GSNL) is thanked for his support in every aspect of the work. Anne-Aurélie Sappin from the GSC and Dave Corrigan, formerly from the GSC, are thanked for their liaison between the GSC and GSNL. Dylan Goudie provided assistance with the SEM analyses of thin sections. NR is grateful for the support and assistance of the staff of the Geochronology Laboratories of the Geological Survey of Canada. In particular, Ray Chung, Greg Case and Tom Pestaj are thanked for their careful efforts and excellent work. Matt Polivchuk provided the necessary high-quality zircon SEM images. The manuscript was improved by careful reviews by John Hinchey (GSNL) and Natasha Wodicka (GSC). This is Natural Resources Canada Contribution Number 20230367.

REFERENCES

Black, L.P., Kamo, S.L., Allen, C.M., Davis, D.W., Aleinikoff, J.N., Valley, J.W., Mundil, R., Campbell, I.H., Korsh, R.J., Williams, I.S. and Foudoulis, C.
2004: Improved $^{206}Pb/^{238}U$ microprobe geochronology by monitoring of a trace-element-related matrix effect; SHRIMP, ID-TIMS, ELA-ICP-MS and oxygen isotope documentation for a series of zircon standards. Chemical Geology, Volume 205, pages 115-140.

Bodorkos, S., Bowring, J. and Rayner, N.
2020: Squid3: Next-generation data processing software for Sensitive High Resolution Ion Micro Probe (SHRIMP). Exploring for the Future: Abstracts. Geoscience Australia. https://doi.org/10.11636/133870

Christiansen, E.H. and Keith, J.D.
1996: Trace element systematics in silicic magmas: a metallogenic perspective. *In* Trace Element Geochemistry of Volcanic Rocks: Applications for Massive Sulphide Exploration. *Edited by* D.A. Wyman. Geological Association of Canada, Short Course Notes, Volume 12, pages 115-151.

Ciuculescu, T., Masun, K.M., Weir, I., Vasquez, L. and Goode, J.R.
2022: Technical report on the Deep Fox and Foxtrot Project, Newfoundland and Labrador, Canada. NI 43-101 for Search Minerals Inc., SLR Consulting (Canada) Ltd., 281 pages.

Crocker, M.G.
2014: A Petrographic, Geochemical and Geochronological Study of Rare Earth Mineralization in the Red Wine Intrusive Suite, Labrador, Canada. Unpublished M.Sc. thesis, Memorial University of Newfoundland, 766 pages.

Davis, W.J., Pestaj, T., Rayner, N. and McNicoll, V.M.
2019: Long-term reproducibility of $^{207}Pb/^{206}Pb$ age at the GSC SHRIMP lab based on the GSC Archean reference zircon z1242. Geological Survey of Canada, Scientific Presentation 111, 1 poster. https://doi.org/10.4095/321203

Dostal, J.
2016: Rare metal deposits associated with alkaline/peralkaline igneous rocks. Reviews in Economic Geology, Volume 18, pages 33-54.

Ducharme, T.A., McFarlane, C.R.M., van Rooyen, D. and Corrigan, D.
2021: Petrogenesis of the peralkaline Flowers River Igneous Suite and its significance to the development of the southern Nain Batholith. Geological Magazine, Volume 168, pages 1911-1936.

Finch, C., Roldan, R., Walsh, L., Kelly, J. and Amor, S.
2018: Analytical methods for chemical analysis of geological materials. Government of Newfoundland and Labrador, Department of Natural Resources, Geological Survey, Open File NFLD/3316, 67 pages.

Förster, H.-J., Tischendorf, G. and Trumbull, R.B.
1997: An evaluation of the Rb *vs.* (Y + Nb) discrimination diagram to infer tectonic setting of silicic igneous rocks. Lithos, Volume 40, pages 261-293. https://doi.org/10.1016/S0024-4937(97)00032-7

Goode, J.R.
2021: The extractive metallurgy of Rare Earth Elements. PEGNL Professional Short Course: Critical Minerals and Net Zero. Presentation at Mineral Resources Review, CIM NL Branch, St. John's.

Gower, C.F.
2010a: Bedrock geological maps for the Grenville Province and adjacent Makkovik in eastern Labrador. Government of Newfoundland and Labrador, Department of Natural Resources, Geological Survey, Maps 2010-01 to 2010-25, 1:100 000 scale.

2010b: Geology of the Grenville Province and adjacent eastern Makkovik Province, eastern Labrador. Government of Newfoundland and Labrador, Department of Natural Resources, Geological Survey, Map 2010-50, scale 1:500 000.

2019: Regional geology of eastern Labrador (eastern Makkovik and Grenville provinces). Government of Newfoundland and Labrador, Department of Natural Resources, Geological Survey, Memoir 4, 654 pages.

Haley, J.T.
2014: 1.3 Ga Bimodal Volcanism in Southeastern Labrador: Fox Harbour. Unpublished M.Sc. thesis, Memorial University of Newfoundland, St. John's, Newfoundland, 209 pages.

Hughes, C.J.
1973: Spilites, keratophyres, and the igneous spectrum. Geological Magazine, Volume 109, pages 513-527.

Ludwig, K.
2012. User's manual for Isoplot/Ex rev. 3.70: A Geochronological Toolkit for Microsoft Excel. Special Publication, 5, Berkeley Geochronology Center, Berkeley, 76 pages.

Magyarosi, Z.
2023: Geochemical data from the REE mineralized Fox Harbour Volcanic Belt, and the spatially and genetically associated rocks in southeastern Labrador (NTS map areas 3D/04, 05, 13A/08 and 09). Government of Newfoundland and Labrador, Department of Industry, Energy and Technology, Geological Survey, Open File LAB/1784, 8 pages.

Magyarosi, Z. and Rayner, N.
2023: Petrography, geochemistry and geochronology of the REE-mineralized Fox Harbour Volcanic Belt, southeastern Labrador. In Current Research. Government of Newfoundland and Labrador, Department of Industry, Energy and Technology, Geological Survey, Report 23-1, pages 47-75.

Miller, R.R.
2015: Pantellerite-hosted rare earth element mineralization in southeast Labrador: The Foxtrot deposit. In Symposium on Strategic and Critical Materials Proceedings. *Edited by* G.J. Simandl and M. Neetz. British Columbia Ministry of Energy and Mines, British Columbia Geological Survey, Paper 2015-3, pages 109-117.

Miller, R.R., Heaman, L.M. and Birkett, T.C.
1997: U-Pb zircon age of the Strange Lake peralkaline complex: Implications for Mesoproterozoic peralkaline magmatism in north-central Labrador. Precambrian Research, Volume 81, pages 67-82.

Müller, A., Reimer, W., Wall, F., Williamson, B., Menuge, J., Brönner, M., Haase, C., Brauch, K., Pohl, C., Lima, A., Teodoro, A., Cardoso-Fernandes, J., Roda-Robles, E., Harrop, J., Smith, K., Wanke, D., Unterweissacher, T., Hopfner, M., Schröder, M., Clifford, B., Moutela, P., Lloret, C., Ranza, L. and Rausa, A.
2023: GREENPEG – exploration for pegmatite minerals to feed the energy transition: first steps towards the Green Stone Age. In The Green Stone Age: Exploration and Exploitation of Minerals for Green Technologies. *Edited by* M. Smelror, K. Hanghøj and H. Schiellerup. Geological Society, London, Special Publication 526, pages 193-218.

Pearce, J.A., Harris, N.B.W. and Tindle, A.G.
1984: Trace element discrimination diagrams for the tectonic interpretation of granitic rocks. Journal of Petrology, Volume 25, pages 956-983. https://doi.org/10.1093/petrology/25.4.956

Shand, S.J.
1922: The problem of the alkaline rocks. Proceedings of the Geological Society of South Africa, Volume 25, pages 19-33.

Spitz, G. and Darling, R.
1978: Major and minor element lithogeochemical anomalies surrounding the Louvem copper deposit, Val d'Or, Quebec. Canadian Journal of Earth Sciences, Volume 15, pages 1161-1169.

Stacey, J.S. and Kramers, J.D.
1975: Approximation of terrestrial lead isotope evolution by a two-stage model. Earth and Planetary Science Letters, Volume 26, pages 207-221.

Steiger, R.H. and Jäger, E.
1977: Subcommission on geochronology; Convention on the use of decay constants in geo- and cosmochronology. Earth and Planetary Science Letters, Volume 36, pages 359-362.

Stern, R.A.
1997: The GSC Sensitive High Resolution Ion Microprobe (SHRIMP): analytical techniques of zircon U-Th-Pb age determinations and performance evaluation. *In* Radiogenic Age and Isotopic Studies. Report 10, Geological Survey of Canada, Current Research 1997-F, pages 1-31.

Stern, R.A. and Amelin, Y.
2003: Assessment of errors in SIMS zircon U-Pb geochronology using a natural zircon standard and NIST SRM 610 glass. Chemical Geology, Volume 197, pages 111-146.

Sun, S.S. and McDonough, W.F.
1989. Chemical and isotopic systematics of oceanic basalts: implications for mantle composition and processes. *In* Magmatism in the Ocean Basins. *Edited by* A.D. Saunders and M.J. Norry. Geological Society of London, Special Publication 42, pages 313-345.

Vasyukova, O.E. and Williams-Jones, A.E.
2018: Direct measurement of metal concentrations in fluid inclusions, a tale of hydrothermal alteration and REE ore formation from Strange Lake, Canada. Chemical Geology, Volume 483, pages 385-396. https://doi.org/10.1016/j.chemgeo.2018.03.003

Whalen, J.B., Currie, K.L. and Chappell, B.W.
1987: A-type granites: geochemical characteristics, discrimination and petrogenesis. Contributions to Mineralogy and Petrology, Volume 95, pages 407-419.

Whalen, J.B. and Hildebrand, R.S.
2019: Trace element discrimination of arc, slab failure, and A-type granitic rocks. Lithos, Volumes 348-349, 105179. https://doi.org/10.1016/j.lithos.2019.105179

Whitney, D.L.
2010: Abbreviations for names of rock-forming minerals. American Mineralogist, Volume 95, pages 185-187.

Wilson, M.
1989: Igneous Petrogenesis: A Global Tectonic Approach. Chapman Hall, London, 466 pages. https://doi.org/10.1180/minmag.1989.053.372.15

Wise, M.A., Müller, A. and Simmons, W.B.
2022: A proposed new mineralogical classification system for granitic pegmatites. The Canadian Mineralogist, Volume 60, pages 229-248.